(12) INTERNATIONAL APPLICATION PUBLISHED UNDER THE PATENT COOPERATION TREATY (PCT)

(19) World Intellectual Property Organization
International Bureau

(43) International Publication Date
02 January 2020 (02.01.2020)

WIPO | PCT

(10) International Publication Number
WO 2020/005768 A1

(51) International Patent Classification:
B82Y 15/00 (2011.01) *G01N 33/543* (2006.01)
G01N 33/50 (2006.01)

(21) International Application Number:
PCT/US2019/038539

(22) International Filing Date:
21 June 2019 (21.06.2019)

(25) Filing Language: English

(26) Publication Language: English

(30) Priority Data:
62/689,455 25 June 2018 (25.06.2018) US

(71) Applicant: **THE REGENTS OF THE UNIVERSITY OF CALIFORNIA** [US/US]; 1111 Franklin Street, Twelfth Floor, Oakland, California 94607-5200 (US).

(72) Inventors: **DI CARLO, Dino**; 10889 Wilshire Blvd., Suite 920, Los Angeles, California 90095-7191 (US). **OUYANG, Mengxing**; 10889 Wilshire Blvd., Suite 920, Los Angeles, California 90095-7191 (US).

(74) Agent: **DAVIDSON, Michael S.**; Vista Ip Law Group LLP, 100 Spectrum Center Drive, Suite 900, Irvine, California 92618 (US).

(81) Designated States *(unless otherwise indicated, for every kind of national protection available)*: AE, AG, AL, AM, AO, AT, AU, AZ, BA, BB, BG, BH, BN, BR, BW, BY, BZ, CA, CH, CL, CN, CO, CR, CU, CZ, DE, DJ, DK, DM, DO, DZ, EC, EE, EG, ES, FI, GB, GD, GE, GH, GM, GT, HN, HR, HU, ID, IL, IN, IR, IS, JO, JP, KE, KG, KH, KN, KP, KR, KW, KZ, LA, LC, LK, LR, LS, LU, LY, MA, MD, ME, MG, MK, MN, MW, MX, MY, MZ, NA, NG, NI, NO, NZ, OM, PA, PE, PG, PH, PL, PT, QA, RO, RS, RU, RW, SA,

(54) **Title:** PLASMONIC SWARM BIOSENSING SYSTEM AND METHODS OF USE

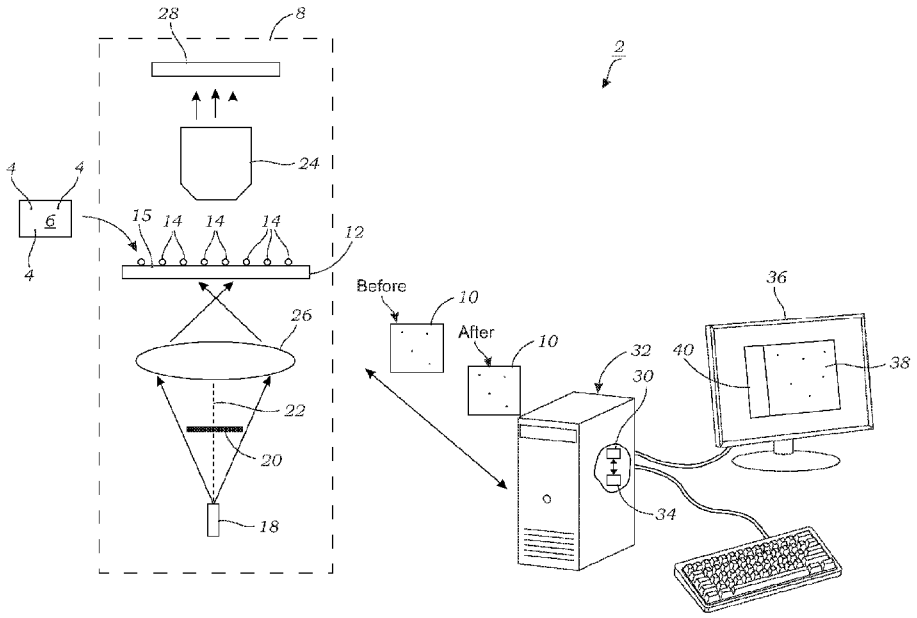

FIG. 1

(57) **Abstract:** A system for determining the presence and/or concentration of an analyte in a sample includes an optically transparent substrate having a plurality of plasmonic nanoparticles immobilized thereon and a dark field imaging device configured to acquire color images of the optically transparent substrate before and after exposure to the analyte. Image processing software is configured to define regions of interest (ROIs) in the acquired color images that represent individual plasmonic nanoparticles, wherein the image processing software is further configured to extract color intensity values from one or more color channels from each ROI to calculate a hue value for individual plasmonic particles before and after exposure to the analyte. A delta hue value is calculated from the respective before and after hue values for the individual plasmonic nanoparticles which is used to determine the presence and/or concentration of the analyte.

WO 2020/005768 A1

[Continued on next page]

SC, SD, SE, SG, SK, SL, SM, ST, SV, SY, TH, TJ, TM, TN, TR, TT, TZ, UA, UG, US, UZ, VC, VN, ZA, ZM, ZW.

(84) **Designated States** *(unless otherwise indicated, for every kind of regional protection available)*: ARIPO (BW, GH, GM, KE, LR, LS, MW, MZ, NA, RW, SD, SL, ST, SZ, TZ, UG, ZM, ZW), Eurasian (AM, AZ, BY, KG, KZ, RU, TJ, TM), European (AL, AT, BE, BG, CH, CY, CZ, DE, DK, EE, ES, FI, FR, GB, GR, HR, HU, IE, IS, IT, LT, LU, LV, MC, MK, MT, NL, NO, PL, PT, RO, RS, SE, SI, SK, SM, TR), OAPI (BF, BJ, CF, CG, CI, CM, GA, GN, GQ, GW, KM, ML, MR, NE, SN, TD, TG).

Published:

— *with international search report (Art. 21(3))*

PLASMONIC SWARM BIOSENSING SYSTEM AND METHODS OF USE

Related Application

[0001] This Application claims priority to U.S. Provisional Patent Application No. 62/689,455 filed on June 25, 2018, which is hereby incorporated by reference. Priority is claimed pursuant to 35 U.S.C. § 119 and any other applicable statute.

Technical Field

[0002] The technical field generally relates to systems and methods that utilize localized surface plasmon resonance (LSPR) which measures the collective electron charge oscillations in metallic nanoparticles excited by light. More specifically, the technical field relates to a system and method that examines the hue shift of large numbers of individual nanoparticles that result from the binding/interaction with a target chemical species or analyte. The system uses a dark field imaging setup to detect the location of individual nanoparticles and analyze the respective hue shifts in response to exposure to an analyte.

Statement Regarding Federally Sponsored Research and Development

[0003] This invention was made with government support under Grant Number 1648451, awarded by the National Science Foundation. The government has certain rights in the invention.

Background

[0004] Nanoplasmonic sensors have become a promising solution for sensing of bio-analytes. Due to strong light localization, these nanosensors are sensitive to even a few molecules that when bound to their surface perturb the electromagnetic field distribution. Indeed, detection sensitivity down to a single molecule level has been demonstrated. Despite the significant progress in the development of nanoplasmonic biosensors, few of these approaches have yet to reach commercial products for point-of-care diagnostics. The main hurdles are associated with achieving both compact instrumentation and robust sensing performance for practical use. In general, biosensing measurements are affected by variability in surface properties in different devices, the imperfections in manufacture of sensing elements, biological noise such as non-specific binding, and measurement noise introduced by the readout system, which together lead to systematic and random errors. For

biosensing applications from clinical samples, the sensor performance is further negatively affected by the matrix effect in biofluids, causing reduced target binding and elevated background noise.

[0005] Conventional nanoplasmonic detection schemes typically measure the collective signal from an ensemble of nanosensors which yields an averaged sensor readout as a single measurement, where the properties of individual particles remain unseen within an integrated spectrum. Many recent nanoplasmonic sensors have been reported using ensemble signals for biomarker detection in biofluids, such as spectral shift, intensity, and area ratio with maximum brightness. An ensemble measurement not only loses information from individual nanosensors and compromises the detection sensitivity, but also introduces random noise due to the lack of repeated measurements on the same sample. In bulk measurements, particle size variation may broaden the spectral signature and reduce detection resolution, which cannot be efficiently improved even when averaged spectral shifts is used as an output. On the other hand, measuring signal shifts of single nanoparticles allows the examination of particle variation and the minimization of systematic error at single particle resolution, which cannot be achieved using bulk measurements. Sensing with single nanoparticles providing individual readouts has been explored, but spectral imaging on a large number of particles requires bulky and expensive setups for hyperspectral imaging, otherwise only low throughput ($n \leq 120$) has been achieved with manual interrogation. All these factors hinder the adoption of nanoplasmonic sensors for point-of-care applications.

[0006] Individual nanoplasmonic sensors can also have variable readouts. Because the nanoplasmonic effect is a near-field phenomenon, only binding events that occur at tens of nanometers around the sensor surface will affect the sensor signal. Therefore, the matrix effect and bulk background noise is greatly suppressed. However, these nanosensors (with critical dimensions from 40-100 nm) have limited binding sites on their surface (typically 100-1000 binding sites). As a result, when the analyte concentration is much lower than the affinity of the capture antibody being used, the dynamic binding process leads only to a small fraction of bound analyte-antibody states. For example, at low analyte concentration of ~10 pM, only ~1/10 to 1/100 of surface antibodies are converted to bound states based on the Langmuir adsorption model, assuming a typical affinity for antibody-antigen pairs of 100 pM - 1 nM. Therefore, an individual nanosensor only captures on the order of 10 molecules. In addition, plasmonic nanosensors have highly inhomogeneous optical field distributions. Therefore, the sensor signal strongly depends on the location where the analyte is bound on

the sensor surface with respect to the direction of optical excitation. These, taken together, introduce a large statistical uncertainly in optical signal among individual nanosensors.

Summary

[0007] In one embodiment, a swarm biosensing platform is disclosed with an alternative detection scheme, where the output from each single nanoparticle "sensor" is collected and compared to its initial state (i.e., before and after comparisons are made). The distribution of these individual sensor "votes" from multiple nanoparticle sensors can then be automatically characterized by image processing software to determine a reliable sensing result with high statistical probability to represent its true value. Specifically, for plasmonic sensing, the sensing substrate is composed of a multitude of single plasmonic nanoparticles spread over an optically transparent surface which can be individually interrogated. However, instead of measuring spectral shift from the average of many scattering nanoparticles in solution or the final state of an assembly of nanoparticles on a surface, a color camera is used to monitor the hue change of the individual nanoparticles by extracting the RGB information for each nanoparticle from dark field images which is then converted to hue values. A few hundred to over a thousand single nanoparticles are interrogated within one imaging field of view (FOV) (172 μm × 122 μm), leading to thousands of single nanoparticles per sample, enabling statistical analysis of sensing outputs from a large number of sensors for each device.

[0008] In one particular implementation, detector nanoparticles were also used to amplify the color or hue shift, which has proven to yield 3 to 7-fold enhanced spectral shift in conventional spectrum-based detection. This signal amplification permits the platform to achieve good sensitivity (~pM) without the need of recovering the spectrum information, thus keeping the setup compact and low-cost. In addition, the swarm sensing platform exhibited a large dynamic range (> 4 orders of magnitude), and high quantitation ability to reliably differentiate three clinically relevant c-reactive protein (CRP) concentrations (in a narrow range of 1-10 μg/ml) in human serum. Compared with conventional approaches that rely on averaged signal from a localized ensemble of particles without correlation at the single-particle level, the swarm sensing platform and methods recognize individual signal shifts from a large population of single nanoparticles, and therefore achieves more consistent sensor readouts despite particle or device variations. These key features will allow adaptation or use of the platform for nanoplasmonic point-of care assays, where robust quantitative readout in a small form factor is critical for use in rapid turnaround time tests in clinical or community health settings.

[0009] In one embodiment, a system for determining the presence and/or concentration of an analyte in a sample includes an optically transparent substrate having a plurality of plasmonic nanoparticles immobilized on a surface thereof. The system includes a dark field imaging device configured to acquire color images of the optically transparent substrate before and after exposure to the analyte and image processing software configured to define regions of interest (ROIs) in the acquired color images, the ROIs representing individual plasmonic nanoparticles, wherein the image processing software is further configured to extract color intensity values from one or more color channels from each ROI to calculate a hue value for individual plasmonic particles before and after exposure to the analyte, wherein the image processing software calculates a delta hue value from the respective before and after hue values for the individual plasmonic nanoparticles and wherein the presence and/or concentration of the analyte is based on the delta hue values of the plasmonic nanoparticles.

[0010] In another embodiment, a method for determining the presence and/or concentration of an analyte in a sample includes providing an optically transparent substrate having a plurality of plasmonic nanoparticles immobilized on a surface thereof; imaging the optically transparent substrate before the sample has been applied with a dark field imaging device configured to acquire one or more before color images of the optically transparent substrate; loading the optically transparent substrate with the sample; imaging the optically transparent substrate after the sample has been applied with a dark field imaging device configured to acquire one or more after color images of the optically transparent substrate; and subjecting the respective before and after color images to image processing software configured to define regions of interest (ROIs) in the respective before and after color images, the ROIs representing individual plasmonic nanoparticles, wherein the image processing software is further configured to extract color intensity values from one or more color channels from each ROI to calculate a hue value for individual plasmonic particles in the respective before and after color images, wherein the image processing software calculates a delta hue value from the respective before and after hue values for the individual plasmonic particles and wherein the presence and/or concentration of the analyte is based on the delta hue values of the plasmonic nanoparticles.

[0011] In another embodiment, a system for determining the presence and/or concentration of an antibody in a sample includes an optically transparent substrate having a plurality of plasmonic nanoparticles immobilized on a surface thereof and conjugated to an analyte specific for the antibody. The system further includes a dark field imaging device configured to acquire color images of the optically transparent substrate before and after

exposure to the antibody and image processing software configured to define regions of interest (ROIs) in the acquired color images, the ROIs representing individual plasmonic nanoparticles, wherein the image processing software is further configured to extract color intensity values from one or more color channels from each ROI to calculate a hue value for individual plasmonic particles before and after exposure to the antibody, wherein the image processing software calculates a delta hue value from the respective before and after hue values for the individual plasmonic nanoparticles and wherein the presence and/or concentration of the antibody is based on the delta hue values of the plasmonic nanoparticles.

Brief Description of the Drawings

[0012] FIG. 1 schematically illustrates a system for determining the presence and/or concentration of a particular chemical species or analyte in a sample according to one embodiment.

[0013] FIGS. 2A and 2B illustrate UV-Vis results of direct binding. A series of anti-BSA (200 μM) solutions were added to the cuvette containing 500 μL of gold nanoparticle (AuNP) solution sequentially at 2 min intervals, followed by an immediate spectral measurement after each addition. The volume of anti-BSA added was 1 μL over 5 times, and lastly 5 μL for the binding to reach saturation. FIG. 2A illustrates the normalized absorbance spectrums. Increasing amounts of anti-BSA antibody lead to a redshift in the wavelength of the peak signal (arrow A); FIG. 2B illustrates peak wavelength and absorbance of bare AuNPs, conjugated AuNPs, and each step during direct binding. Slight decreases in peak absorbance after conjugation and final washing steps at the end of direct binding experiments demonstrate good AuNPs recovery rate.

[0014] FIG. 3 illustrates a schematic of the system for determining the presence and/or concentration of a particular chemical species in a sample that uses a plurality or swarm of single nanoparticle colorimetric sensors. The spectral shifts due to the binding of sandwiched AuNP pairs correlates with a detectable hue shift of the individual nanoparticles using a color image sensor. Analyte detection is performed as follows: Capture AuNPs conjugated with analyte-specific ligand are first immobilized and a "before" image is taken to record each individual sensor's initial hue. Next, target analyte and detector AuNPs were added sequentially, incubated on-chip, and washed. Finally, the "after" sensing image was taken at the same location to record the final resulting hue. The change in hue (i.e., delta hue) of each individual nanoparticle was compiled to generate a histogram representing the sensor readout.

[0015] FIG. 4 illustrates a sample image of region of interest (ROI) selection using an automated imaging algorithm performed by image processing software. Circle outlines represent the ROIs selected.

[0016] FIG. 5 illustrates a table showing screening candidates for capture gold nanoparticles.

[0017] FIG. 6 illustrates a table showing screening candidates for detector gold nanoparticles.

[0018] FIG. 7 illustrates simulation of delta hue changes with number of detector probes (10nm AuNPs) bound to a capture probe (100nm AuNP). Interparticle distances of 5, 10 and 15nm were used. The simulation assumed that only a single layer of detector probes was formed, and there was no overlap between adjacent detector probes. The maximum number of 10nm AuNPs attached to a 100nm AuNP probe was estimated to be 107, 75, and 57 if the antibody conjugation layer was 5, 10 and 15nm thick respectively.

[0019] FIGS. 8A and 8B illustrate the evaluation of HSV components besides hue -- saturation and value using CRP detection in buffer solution (FIG. 8A) and human serum (FIG. 8B).

[0020] FIGS. 9A and 9B illustrate respective graphs of particle fraction as a function of RGB intensity shifts (FIG. 9A) and hue shifts (FIG. 9B) due to conjugation, direct binding and detector AuNP binding in a colloidal state. Different nanoparticle states and controls are illustrated on the right side of FIGS. 9A and 9B. AuNP solutions after each step were added onto a glass coverslip, dried, and then imaged in darkfield. Histograms of hue for individual particles show significant changes in hue are visible. The capture probe and detector probe used in this experiment were AuNPs with 100 and 20 nm diameter.

[0021] FIG. 10A illustrates a histogram of particle fraction as a function of delta hue for different concentrations of anti-BSA.

[0022] FIG. 10B illustrates a graph of mean delta hue as a function of anti-BSA concentration. In the control group, DI water was added instead of antibody solution, followed by detector AuNPs. The error bars represent standard error σ_n of each device, which is calculated by $\sigma_n = \sigma/\sqrt{n}$, where σ is the standard deviation of the population, and n is the sample size. For all groups, sample size $n > 1100$ single nanoparticles.

[0023] FIG. 10C illustrates a histogram of particle fraction as a function of delta hue for different concentrations of CRP.

[0024] FIG. 10D illustrates a graph of mean delta hue as a function of CRP concentration. In the control group, DI water was added instead of antibody solution, followed by detector AuNPs. The error bars represent standard error σ_n of each device, which is calculated by $\sigma_n = \sigma/\sqrt{n}$, where σ is the standard deviation of the population, and n is the sample size. For all groups, sample size $n > 1100$ single nanoparticles.

[0025] FIG. 11A illustrates stacked histograms of particle fraction as a function of delta hue at different CRP concentrations. Stacked histograms are pooled from three separate experiments, with each shading representing a different experiment.

[0026] FIG. 11B illustrates a graph of mean delta hue as a function of CRP concentration. The error bars represent the standard deviation of the mean value of the nanoparticle swarm from three devices. In the control group, CRP-free serum was added instead of CRP antibody solution, followed by detector AuNPs. p-values were determined by two-tailed student t-tests. * $p < 0.05$, ** $p < 0.01$. For all groups, sample size $n > 2000$.

[0027] FIG. 12 is a graph of mean delta hue for two concentrations of CRP spiked in serum using a commercial blocking buffer compared to without use of the blocking buffer.

[0028] FIG. 13 illustrates a graph of normalized standard error versus sample size of swarm sensors for CRP detection in buffer at different concentrations.

[0029] FIG. 14A illustrates a histogram of different numbers (n) as a function of after-hue values of swarm nanoparticles at different concentrations of anti-BSA (analyte) in water using after-hue as readout.

[0030] FIG. 14B illustrates the mean after hue values versus anti-BSA concentration. Dotted line represents the control group. In the control group, DI water was added instead of antibody solution, followed by detector AuNPs. The error bars in FIG. 14B represent standard error σ_n of each device. which is calculated by $\sigma_n = \sigma/\sqrt{n}$, where σ is the standard deviation of the population, and n is the sample size. N indicates the number of nanoparticle sensors interrogated. Compared to the same set of data using delta hue as readout, these results using after hue show less quantitative accuracy because of systematic error in the before hue of sensors in a set of experiments.

[0031] FIG. 15A illustrates a histogram of nanoparticle fraction for after hue values for nanoparticles used with different concentrations of CRP spiked in human serum. Stacked histograms are pooled from three separate experiments, with each color representing a different experiment.

[0032] FIG. 15B illustrates a graph of mean value of after hue as a function of CRP concentration. The error bars in FIG. 15B represent the standard deviation of the mean value of the nanoparticle swarm from three devices. In the control group, CRP-free serum was added instead of CRP antibody solution, followed by detector AuNPs. *p*-values were determined by two-tailed student *t*-tests. * $p < 0.05$, ** $p < 0.01$. For all groups, sample size $n > 2000$. Compared to the same set of data using delta hue as readout, these results using after hue show less quantitative accuracy because of systematic error in the before hue of sensors in a set of experiments.

[0033] FIG. 16A is a scatter plot of delta hue versus before hue concentration for anti-BSA in DI water at 100 nM. Each point in the scatter plot represents a single nanoparticle from the swarm. The histogram above the scatter plot indicates the before-hue distribution for each group.

[0034] FIG. 16B is a scatter plot of delta hue versus before hue concentration for CRP in DI water at 10 μg/ml (i.e., 87 nM). The histogram above the scatter plot indicates the before-hue distribution for each group.

[0035] FIG. 16C is a scatter plot of delta hue versus before hue concentration for CRP spiked in serum at 10 μg/ml. The histogram above the scatter plot indicates the before-hue distribution for each group.

[0036] FIG. 17A illustrates a scatter plot of delta hue versus before hue at different concentrations for BSA in DI water.

[0037] FIG. 17B illustrates a scatter plot of delta hue versus before hue at different concentrations for CRP in DI water.

[0038] FIG. 17C illustrates a scatter plot of delta hue versus before hue at different concentrations for CRP in serum.

Detailed Description of Illustrated Embodiments

[0039] FIG. 1 illustrates a system 2 for determining the presence and/or concentration of a particular chemical species 4 in a sample 6 according to one embodiment. The chemical species may include an analyte that may be, by way of example, a protein, protein fragment, nucleic acid, microRNA, antigen, drug, drug metabolite, biomolecule, virus, exosome/microvesicle or the like. In some embodiments, the chemical species 4 is an antibody (as opposed to the antigen). The sample 6 may include a biological sample such as a bodily fluid obtained from a living mammal. Examples of such fluids include blood, blood plasma, blood serum, pleural fluid, peritoneal fluid, semen, saliva, sweat, tears, and the like.

The sample 6 may, in some embodiments, be subject one or more sample preparation operations prior to being tested in the system. Sample preparation operations may include filtration, separation, centrifugation, concentration, dilution, preservation, and other sample preparation operations that are conventionally known to those skilled in the art.

[0040] As seen in FIG. 1, the system 2 includes a dark field imaging device 8 that is used to obtain "before" and "after" color images 10 of an optically transparent substrate 12 having a plurality of plasmonic nanoparticle sensors 14 (also referred to herein as nanoparticles, NPs, or AuNPs for gold nanoparticles) that are located at fixed positions (i.e., immobilized) on the optically transparent substrate 12. Nanoparticles 14 refers to nanometer-sized particles that exhibit surface plasmon resonance. Nanoparticles 14 may include any number of shapes of particles including by way of example, nanospheres, nanorods, nanostars, and other morphologies. For nanospheres, in one particular embodiment, the nanoparticles 14 can be made of a plasmonic enhancing material (or coated with) such as silver or gold. The particular size of the nanoparticles 14 may also vary. In one embodiment, the nanoparticles 14 are nanospheres and have diameters within the range of about 60-150 nm. Gold nanorods 14 with various aspect ratios exhibiting surface plasmon resonance (SPR) wavelength peaks at the range of 500-650 nm may also be used.

[0041] The optically transparent substrate 12 may be formed as part of a microfluidic device or chip that includes at least one optically transparent surface that holds the immobilized nanoparticles 14. Additional layers or surfaces may be combined to form the completed device or chip. For example, the nanoparticles 14 may reside within a channel, well, or reservoir that includes a bottom and top surface (both of which are optically transparent in the regions that hold the nanoparticles 14). The optically transparent substrate 12 may also contain one or more fiducial marks 15 which may be used to locate certain regions of the optically transparent substrate 12. For example, one region of the optically transparent substrate 12 may contain capture nanoparticles 14 that capture a first chemical species 4 while another region of the optically transparent substrate 12 may contain capture nanoparticles 14 that capture a second chemical species 4. The different geographical regions or locations may be identified by fiducial marks 15 (FIG. 1). The fiducial marks 15 may also be used by the image processing software 30 to register before and after images to one another. Likewise, the fiducial marks 15 may be used to register different FOVs into larger FOVs or the like. Formation of fiducial marks may take place using a number of well-known manufacturing techniques, including selective etching of the transparent substrate 12, screen printing, evaporation and etching of a metal layer and other surface patterning techniques.

[0042] As best seen in FIG. 3, the nanoparticles 14 are conjugated to a chemical or biological moiety 16 that binds or otherwise captures or localizes the particular chemical species 4 that is to be detected or measured (e.g., concentration). Examples of chemical or biological moieties 16 include aptamers, oligonucleotides, antibodies, antigens, and the like. These nanoparticles 14 that are immobilized to the optically transparent substrate 12 may be referred to herein as the capture nanoparticles 14. In one particular embodiment, the nanoparticles 14 are conjugated to an antibody 16 that itself binds to an antigen or other chemical species 4. Such conjugation of an antibody 16 (or other molecule or moiety 16) to the nanoparticles 14 may take place using well-known conjugation techniques. An example of such linking chemistry includes carbodiimide crosslinking such as carbodiimide (EDC)/ N-hydroxysuccinimide (NHS) coupling protocols which are well-known to those skilled in the art. In one embodiment, the plurality of nanoparticles 14 that are immobilized to the optically transparent substrate 12 are conjugated or linked to the same molecule or moiety 16 (e.g., the same antibody). However, in other embodiments plurality of nanoparticles 14 that are immobilized to the optically transparent substrate 12 are conjugated or linked to a different molecule or moiety 16. For example, some of the plurality of the nanoparticles 14 may be conjugated with antibody 16 of type #1 while another plurality of nanoparticles 14 may be conjugated with antibody 16 of type #2. This enables the ability of the system 2 to perform multiplex analysis for multiple chemical species (e.g., analytes) at the same time. It should be noted that the number of types of nanoparticles 14 with different moieties 16 is not limited to two and can be larger than two.

[0043] In some embodiments, it is sufficient to generate enough of a hue shift or hue signal (as explained below) in response to the presence of a chemical species of interest (e.g., target) such that only the capture nanoparticles 14 are needed. However, in other embodiments where the signal or hue shift is not as significant, a second plurality of nanoparticles 14 are added with or after target binding to the capture nanoparticles 14. These second plurality of nanoparticles 14 which may be referred to as detector nanoparticles 14 may conjugate or link with the captured or bound chemical species 4 found on the capture nanoparticles 14. For example, the detector nanoparticles 14 may be conjugated to another antibody specific to another epitope on the bound chemical species 4 separate from the epitope by which it is bound to the capture nanoparticle 14 through moiety 16 (e.g., monoclonal antibody pairs) that amplify the plasmonic signal from the capture nanoparticles 14 (as seen in FIG. 3). In some instances, the detector nanoparticles 14 may be conjugated with a fluorescent probe, dye, or reporter molecule/moiety such that a fluorescent signal may

also be emitted along with the hue shift. In this regard, a fluorescent probe is co-located with some of the nanoparticles 14. In another embodiment, the detector nanoparticles 14 are generally smaller than the capture nanoparticles 14 as seen in FIG. 3. For example, in one particular embodiment, the capture nanoparticles 14 may have a major dimension (or diameter) that is on the order of about 100 nm while the detector nanoparticles 14 have a major dimension (or diameter) that is on the order of about 10 nm (an about 10x difference in size).

[0044] As explained previously, a dark field imaging device 8 is used to obtain both "before" and "after" color images 10 of the optically transparent substrate 12 with the immobilized plurality of nanoparticles 14 located on the surface thereof. Dark field imaging devices 8 are well known in the art. With reference to FIG. 1, the dark field imaging device 8 generally includes a light source 18 along with a dark field obstruction 20 (e.g., annulus or disc) that is positioned along the optical path 22 that prevents direct or non-scattered light from entering an objective lens 24. One or more lenses 26 (e.g., condenser lens) are positioned on an opposing side of the dark field obstruction 20 that serve to illuminate the optically transparent substrate 12 (with or without the sample 6). Light that is scattered by the sample 6/nanoparticles 14 enter the objective lens 24 while direct light or non-scattered light does not enter the objective lens 24. The light collected by the objective lens 24 is then imaged with an image sensor 28 such as a CMOS imaging sensor 28 or the like. A generally dark image is captured with bright, colored objects (in this case the nanoparticles 14) being seen. Other imaging approaches, e.g., using oblique illumination such that the illuminating light is aligned to not directly enter the imaging sensor 28 can also be used to image the scattered light from the nanoparticles 14.

[0045] As explained herein, the hue of the colored bright spots located at where the plurality of nanoparticles 14 are present on the optically transparent slide 12 changes in response to the presence and/or concentration of the target chemical species 4 interacting/binding with the nanoparticles 14. Before and after images are acquired to determine the hue change or delta hue in response to exposure to the chemical species 4. The "before" state refers to the state prior to binding of the target chemical species 4 to the nanoparticle 14 (either directly to the capture nanoparticle 14 or through a secondary detector nanoparticle 14). Conversely, the "after" state refers to the state after the target chemical species 4 (and optional detector nanoparticle(s)) 14 are bound to the capture nanoparticle(s) 14. The dark field imaging device 8 obtains color images 10 of the plurality of nanoparticles 14 in the before and after state. The color images 10 are saved or stored as image files (e.g.,

TIFF, JPEG, BMP, RAW, etc.) which are then processed using image processing software 30 contained in a computing device 32 having one or more processors 34. The computing device 32 may include any number of types of computing devices 32 including a personal computer, laptop, tablet PC, or even mobile computing devices such as a Smartphone. The computing device 32 that runs the image processing software 30 may be separate from or integrated/associated with the dark field imaging device 8.

[0046] A number of color images 10 may need to be acquired by the dark field imaging device 8 to cover the entire surface of the optically transparent substrate 12. In this regard, the dark field imaging device 8 may, in some embodiments, scan the surface of the optically transparent substrate 12 to obtain multiple images that can then be combined together to obtain a larger FOV. This may involve movement of the optically transparent substrate 12, movement of optics of the dark field imaging device 8, or both.

[0047] The image processing software 30 is configured to define regions of interest (ROIs) in the before and after color images 10, the ROIs representing individual plasmonic nanoparticles 14 located on the optically transparent substrate 12. Regions of brightness may be used to identify individual nanoparticles 14. Overlapping signal among neighboring nanoparticles 14 may be eliminated automatically from the data pool by the image processing software 30 using parameters such as circularity and area. The before and after color images 10 are analyzed from the same FOV using the image processing software 30. The image processing software 30 is further configured to extract mean red (R), green (G), and blue (B) values from each ROI to calculate a hue value for each individual plasmonic nanoparticle 14 before and after exposure to the sample 6 (with the chemical species 4). In one embodiment, the red (R), green (G), and blue (B) mean values are converted to HSV in terms of hue, saturation, and value, with the hue value being retained for use as described herein. In particular, the image processing software 30 calculates a delta hue value from the respective before and after hue values for each individual plasmonic nanoparticle 14 using an automatic subtraction operation performed by the image processing software 30. This delta hue data, which is applied to all or a subset of the plurality of particles 14 is obtained by the image processing software 30. The image processing software 30 then uses this delta hue data to determine the presence and/or concentration of the target chemical species 4 within the sample 6. In some embodiments, the delta hue value from only a single color channel is used. In other embodiments, the delta hue values from multiple or all color channels are used. In addition, color channels outside the red, green, or blue wavelengths may also be used in other embodiments. It should also be appreciated that not all nanoparticles 14 need to

be imaged in the before and after states for the method to work (or if imaged they can be discarded from data analysis). Some nanoparticles 14 may have moved, been washed away, become later immobilized. The large number of random immobilized nanoparticle 14 sensors enables accurate overlaying and matching of before and after images.

[0048] To determine the presence and/or concentration of the target chemical species 4, statistical data of delta hue values from a plurality of nanoparticles 14 are used. This may include, for example, a mean or average delta hue value of all the nanoparticles 14. Statistical data may also include, for instance, the distribution of delta hue among the plurality of nanoparticles 14 that are examined. This may look to the fraction % of nanoparticles 14 exhibiting a certain range of delta hue values instead of looking at the overall mean or average. For example, the fraction of nanoparticles 14 in the collective swarm with a delta hue above a threshold delta hue value can be used to correlate to concentration of analyte. For example, it may be empirically determined that if over 40% of the nanoparticles 14 have a delta hue value over 15°, this may correspond to a particular concentration of the target chemical species 4 within the sample 6. Alternatively, a threshold on the number or fraction of nanoparticles 14 with substantially no change in hue (delta hue within the range of -10 to 0°) can provide a metric of concentration, with this fraction decreasing as the concentration of the chemical species 4 increases. The skewness of the histogram of delta hue values for the nanoparticles 14 can also be used as a metric, or other summary statistics or thresholds of the histogram. In addition, the combination of these metrics based on the nanoparticle 14 histogram can provide a multiparametric space in which machine learning (e.g., support vector machines, logistic regression, etc.) can be used to identify a weighting of each the various metrics to optimally develop a diagnostic readout. Preferably the plurality of nanoparticle sensors 14 analyzed to obtain these above-mentioned metrics comprises more than 200 nanoparticles 14 in order to obtain statistically accurate metrics. More preferably the number of nanoparticle sensors 14 in the plurality is at least 2,000.

[0049] The image processing software 30 outputs or generates a result that is used by the user of the system 2. The output may include an indication that the particular target chemical species 4 is present or not in the sample 6 (e.g., yes/no or positive/negative indication). The output may also include, in addition to or as an alternative to an indication of presence a concentration or amount of the chemical species 4 in the sample 6. This may be expressed as a numerical concentration value or range or it may include a qualitative indication of concentration (e.g., low, medium, high, etc.). The output may also include the total of

amount of the chemical species 4 rather than expressed in a concentration value. The output may be presented to the user on a display 36 that is part of or associated with the computing device 32. The display 36 may have a graphical user interface (GUI) 38 that the user uses to view images 10, patient or sample information, statistical data, and any generated output or results for the sample 6. The user may also have the ability to select certain FOVs or ROIs to analyze.

[0050] Experimental

[0051] MATERIALS AND METHODS

[0052] Conjugation of gold nanoparticles.

[0053] Spherical gold nanoparticles 14 (Nanopartz) were centrifuged and resuspended in 1mM 11-mercaptoundecanoic acid (MUA, 450561, Sigma-Aldrich) for reaction overnight. N-(3-Dimethylaminopropyl)-N'-ethylcarbodiimide hydrochloride (EDC, E6383, Sigma-Aldrich) and n-hydroxysuccinimide (NHS, 130672, Sigma-Aldrich) solution was mixed in MES buffer at 1:2 ratio. Gold nanoparticles 14 (also referred to as AuNPs) in MUA solution were centrifuged and resuspended in EDC/NHS (0.1/0.2mM) in 10mM MES buffer and reacted for 30min. The AuNP solution was then centrifuged and resuspended in antigen or antibody solution followed by 2 hours incubation at room temperature. For Anti-BSA detection, 2μM BSA (Sigma) was used for both capture and detector nanoparticles 14. For CRP detection, 0.1mg/ml Anti-CRP antibody C5 (ab8279, Abcam) and C6 (ab8278, Abcam) were used for 100 nm and 10 nm AuNPs, respectively. The final solution was centrifuged and resuspended in DI water for later use.

[0054] Spectra measurements

[0055] A UV-Vis spectrophotometer (GENESYS™ 10S, Thermo Fisher) was used to monitor the spectral shift of gold nanoparticles 14 in colloidal solutions during conjugation. For each measurement, 500 μL of solution was added to the cuvette and measured against blank, i.e., DI water. For direct binding confirmation, a series of anti-BSA (200 μM) solutions were added to the cuvette containing 500 μL of nanoparticles 14 solution sequentially at 2 min intervals, followed by an immediate spectral measurement after each addition. The volume of anti-BSA added was 1 μL over 5 times, and lastly 5 μL for the binding to reach saturation. The resulting solution was then centrifuged and resuspended in DI water to remove unbound molecules and obtain the final measurement.

[0056] Imaging setup and image analysis

[0057] The dark field imaging device 8 was composed of a 60x dark field objective (NA 0.7), dark field condenser (NA 0.85-0.95), and a color camera (DS-Fi3) mounted to an

inverted microscope, all purchased from Nikon. First, an initial image of the immobilized capture nanoparticles 14 in the liquid solution was taken, namely the "before" image. Then, the target chemical species 4 or analyte was added to the surface of the optically transparent substrate 12 and incubated at room temperature followed by a washing step. Next, detector nanoparticles 14 were added to the surface of the optically transparent substrate 12 for another incubation. Excess and unbound detector nanoparticles 14 were washed away, and images of the same locations were taken as "after" images. Both the "before" and "after" color images were taken with cover slip correction when nanoparticles 14 were immersed in liquid solution. Regions of interests (ROIs) were defined in the "before" images to identify each single nanoparticle 14 "sensor" with the hue value of each sensor converted from RGB readout. Spectral overlapping among neighboring nanoparticles 14 were eliminated automatically from the data pool by the imaging analysis algorithm with the use of parameters such as circularity and area. ImageJ image processing software 30 was used to align the "before" and "after" color images from the same FOV, define ROIs of the individual nanoparticles 14 based on a threshold of brightness, and extract the mean R, G, B value from each ROI to calculate the hue value before and after sensing. Parameters such as circularity and area were used to select ROIs representing single nanoparticles 14. Finally, delta hue was determined by subtracting the after-hue value from before-hue value using image processing software 30.

[0058] SEM of AuNPs

[0059] Bare and conjugated nanoparticles 14 colloidal solutions were dispersed on a silicon substrate, dried and imaged using scanning electron microscopy (Supra 40VP SEM, ZEISS) at 10kV.

[0060] Finite-difference time-domain (FDTD) Simulation

[0061] FDTD software from Lumerical Inc. was used to numerically simulate the 3D scattering spectrum of a gold nanoparticle 14. The total-field scatter-field (TFSF) source was used to simulate dark field imaging. A 100nm gold nanoparticle 14 was placed inside the TFSF. The background index was set as 1.3 (for water). A frequency-domain power monitor was placed outside of the TFSF source to collect the scattered signal. In the experimental setup, the numerical aperture (NA) of the objective was 0.7. Therefore, the size of the power monitor (square shaped) was set twice the distance of the monitor from the nanoparticle 14, which resulted in a collection half-angle of 45 degrees. A shell thicknesses of 2.5, 5, 7.5nm, respectively, with refractive index of 1.45 were placed surrounding the nanoparticle 14 to simulate the functionalized antibody layer. The electromagnetic field decay length of the

100nm nanoparticle 14 was estimated to be 20nm. To simulate the binding of 10nm nanoparticles 14 (with shell layer 2.5, 5 and 7.5nm), random positions were generated on the surface of the 100nm nanoparticles 14 with the criteria that the positions generated for each consecutive 10nm nanoparticle 14 has to be non-overlapping with any existing 10nm nanoparticle 14. Otherwise, a new random position was generated, until no new random positions were available to satisfy the non-overlapping condition within 1000 trials. The resonance spectrum obtained from FDTD simulation was converted to RGB values by overlapping with the color-matching functions defined by the International Commission on Illumination (CIE). Then, the RGB values were then converted to the hue value.

[0062] Nanoplasmonic on-chip detection in water

[0063] Gold capture nanoparticles 14 with 100 nm diameters and detector nanoparticles 14 with 10 nm diameters were both conjugated with BSA in a colloidal solution. A glass coverslip (used as the optically transparent substrate 12) was treated with poly-l-lysine (P8920, Sigma-Aldrich) for 10 min and washed three times with DI water and dried. Then, capture nanoparticles 14 were immobilized on the glass coverslip 12. To immobilize, the solution containing capture AuNP-BSA conjugates was added to a microchannel bound to the glass coverslip and incubated for 2 hours followed by washing 3 times to remove excess unbound nanoparticles 14. The before images of immobilized capture nanoparticles 14 were first taken at different locations on the coverslip in DI water. Then, the solution in the microchannel was replaced with anti-BSA (B7276, Sigma-Aldrich) solution and incubated for 15 min at room temperature. This solution was then washed once with DI water and the BSA-conjugated detector nanoparticle 14 solution was added. After a 30 min incubation, the chip was washed 3 times with DI water and a second set of images at previously recorded fields of view were taken, which are defined as "after" images.

[0064] CRP detection in water and serum

[0065] Gold capture nanoparticles 14 with 100 nm diameters and gold detector nanoparticles 14 with 10 nm diameters were conjugated with anti-CRP C5 and C6 (Sigma-Aldrich) in a colloidal solution, respectively. For initial CRP detection tests, DI water was used as a dilution solvent. For detection in serum, CRP (236603, Sigma-Aldrich) was spiked into CRP free serum (Hytest, Netherland) to constitute CRP in serum at concentrations of 1, 3, and 10 μg/ml, respectively. Similar to the detection of anti-BSA in water, the before images of immobilized capture nanoparticles 14 were first taken at different locations on the coverslip 12. Then, solution was replaced with CRP spiked serum and incubated for 15 min. Then, the chip was washed once with DI water and detector nanoparticles 14 were added.

After a 30 min incubation, the chip was washed 3 times with DI water and the "after" images were taken. For CRP detection in serum in which a blocking step was included to compare, a commercial blocking buffer (37584, Thermo Fisher) was used.

[0066] RESULTS

[0067] Chip design and detection scheme

[0068] Gold nanoparticles 14 with diameters of 100 nm were immobilized in a microchannel sandwiched between two glass coverslips which formed the optically transparent substrate 12. Antibodies 16 were functionalized on gold nanoparticles 14 in the colloidal phase before the immobilization step using conventional EDC/NHS methods detailed herein. The UV-Vis spectrum shift was used to verify the above surface functionalization process (FIGS. 2A and 2B). To validate the binding of the chosen antigen and antibody pairs (4, 16), the UV-Vis spectrum shift was further monitored after adding different concentrations of antigens 4 into the antibody functionalized-AuNP colloid solution (FIG. 2B). To minimize the instrument complexity, the swarm biosensing protocol was based on comparing two dark field images on the nanoparticles 14 immobilized on the optically transparent substrate 12 or sensor chip, free from spectroscopic measurement (FIG. 3). An initial image 10 of the immobilized nanoparticles 14 before addition of analyte 4 (i.e., "before" image) was taken using a CMOS color-camera. Next, the sample solution 6 was injected into the microchannel between two cover slips, followed by the injection of detector nanoparticles 14 of much smaller size (typically ~10 nm) that were functionalized with a paired antibody to amplify the protein binding signal on the capture nanoparticles 14. Last, a second dark field image was taken at the same FOV as the "after" image." A sample image of quantitation for each particle after image analysis is shown in FIG. 4. A histogram 50 of the delta hue from all the single nanoparticles 14 or "sensors" was compiled to obtain the representative detection results of one chip (FIG. 3). Total assay time is less than one hour, which includes 10-15 min of target analyte incubation, and 30 min detector probe incubation, imaging acquisition and washing steps.

[0069] Selection of nanoparticle pairs

[0070] The optimal sizes of the paired capture and detector nanoparticles 14 were selected to maximize the hue shifts caused by binding events. Ideal capture nanoparticles 14 would maintain sufficient scattered light intensity to provide a high detection baseline, while detector nanoparticles 14 would exhibit minimal background signal interference without binding. Gold nanoparticles 14 with diameters of 20, 60, 100 and 150 nm were evaluated as

capture probes under the same imaging conditions, where 100 nm and 150 nm particles appeared green and orange, respectively, with high intensity as seen in FIG. 5.

[0071] In addition, the color camera operates at higher quantum efficiency at wavelengths around 550 nm (i.e., correlating with green hue), implying greater signal to noise ratio at this region. Therefore, gold nanoparticles 14 with 100 nm diameter were selected as capture probes. For the detector nanoparticles 14, gold nanoparticles 14 with diameters of 4, 10, 20 and 60 nm were evaluated based on several criteria (FIG. 6). The ideal candidate would be easy to conjugate, yield a low background signal during dark field imaging, and enhance the hue shift when sandwiched with the capture nanoparticles 14. Therefore, smaller gold nanoparticles 14 (<10nm) were not desirable due to technical difficulty during conjugation as they require ultra-high centrifugation speeds as well as their inability to enhance the hue signal when sandwiched to the capture nanoparticle 14. On the other hand, larger gold nanoparticles 14 (>20nm) adhered non-specifically and led to a larger background noise which may interfere with the signal from capture nanoparticles 14. In the end, 10 nm gold nanoparticles 14 were chosen as detector nanoparticles 14 because they were less prone to provide a false positive signal while providing a similar delta hue when compared to sandwiches formed using 20 nm nanoparticles 14. Furthermore, FDTD simulations indicated that 100 nm gold capture nanoparticles 14 allow a maximum number of ~100 detector gold nanoparticles 14 of 10 nm to bind, creating a hue change of up to 14 (FIG. 7). Therefore, each single nanoparticle 14 functions as a quantitative biosensor with a large number of levels in the analog readout.

[0072] Delta hue for individual nanoparticle readout

[0073] RGB and HSV are alternative color models. During data analysis, RGB information acquired from raw color images 10 was converted to HSV in terms of hue, saturation, and value. Hue, which is independent of intensity and saturation, directly correlates with the dominant wavelength, and therefore has been used as an alternative approach to spectral measurement. HSV values range from 0 to 360° but for the gold nanoparticles 14 used herein the color sensing range (green to red) was typically within the range of 0 to 180°. It should be appreciated that other nanoparticle 14 types and sizes generate changes at higher HSV values (e.g., silver-based nanoparticles 14 may be used in the blue range or > 200°). The other two elements of the HSV color space, i.e., saturation and value are susceptible to interference from imaging conditions, and failed to establish correlation with analyte concentrations (see FIGS. 8A and 8B). Therefore, the signal to noise

ratio was significantly enhanced by converting RGB to HSV and using only hue as the quantitative readout.

[0074] The color change using RGB and hue of individual nanoparticles 14 was monitored and analyzed in each consecutive step during the development of swarm sensors (FIGS. 9A and 9B). The 100nm-AuNP-conjugates remained a green hue with a slight decrease (~10º) compared to unconjugated 100nm nanoparticles 14. A drastic shift of hue was demonstrated in the histograms of AuNP-conjugates bound with Anti-BSA as more single nanoparticles 14 exhibited light green/yellow/light orange hues. This hue shift was further enhanced when the detector nanoparticles 14 were added, where the percentage of nanoparticles 14 with yellow/orange/red increased; ~ 40º hue shift for the population on average. Two control conditions were included and showed that neither non-specific binding of bare gold nanoparticles 14 pairs randomly sandwiched with target analytes 4, nor the binding between capture and detector conjugates yielded significant hue shifts on average. The RGB information for each condition (FIG. 9A) provided insights into the cause of the hue shift. The drastic increase in the red channel value and moderate increase in the green channel value contributed to the hue shift from green to orange/red. The blue channel remained relatively constant throughout all groups, suggesting its potential use as a reference during image acquisition.

[0075] Swarm sensor characterization in buffer

[0076] The sensitivity and dynamic range of the system 2 was characterized using two different proteins in buffer solution. The detection of anti-BSA concentrations ranging from 10 pM to 10 μM was demonstrated, which yielded a shift in the delta hue histogram comprising each sensor's individual readout (FIG. 10A). The large sample size of the sensor swarm ($n>2000$ individual nanoparticles 14 that form the sensors for each optically transparent substrate 12) better enabled differentiation between neighboring concentrations ($p<0.05$). The dynamic range using the mean value of the delta hue (FIG. 10B) was six (6) orders of magnitude with a limit of detection of 10 pM. Detection of CRP in DI water from 1 ng/ml to 10 μg/ml revealed a dynamic range of at least four (4) orders of magnitude with the potential to detect even lower concentrations (FIGS. 10C-10D). 1 ng/ml (i.e., 8.7 pM) was chosen as the lower end of detection because it was comparable to the lowest anti-BSA concentration (i.e., 10 pM) tested. Because the clinical cutoffs are in the μg/ml range, the detection of CRP concentrations lower than 1 ng/ml was not pursued. The detection performance could be affected by the variation of protein markers, affinity of the antigen-antibody pair, as well as protein structure and dimension.

[0077] Detection of a cardiac biomarker in serum

[0078] For practical applications, robust and accurate quantitation are essential features for biomarker detection in clinical settings. For example, CRP, a common inflammation marker, has been demonstrated to be valuable at lower concentrations, i.e., < 10 μg/ml, in both primary and secondary cardiovascular prophylaxis as a predictive marker to evaluate the risk of cardiac diseases. According to Centers for Disease Control and Prevention (CDC) guidelines, CRP levels lower than 1 μg/ml, within 1 and 3 μg/ml, and within 3 and 10 μg/ml are classified as low, intermediate and high coronary risks, respectively. The recommendation of this high-sensitivity CRP (hsCRP) assessment for patients with moderate risk of cardiovascular disease has been implemented in several countries in recent years, i.e., American Heart Association and CDC in United States in 2003, Canadian Cardiology Society in 2009, and European Society of Cardiology in 2012. The swarm sensing system 2 was evaluated with hsCRP detection in human serum at clinical cutoffs at 1, 3, and 10 μg/ml. The peak of the stacked histogram shifted to larger delta hue as CRP concentration increased (FIG. 11A). The mean delta hue from three different devices (optically transparent substrates 12) was used to represent the detection output (FIG. 11B) with each of the clinical ranges found to be statistically distinct ($p < 0.05$), demonstrating the ability to successfully differentiate between the three clinical cutoffs with good sensor reproducibility. Furthermore, the results of CRP detection was compared in serum with and without blocking at two clinically relevant concentrations (i.e., 1 and 10 μg/ml), and no significant difference was found (FIG. 12).

[0079] DISCUSSION

[0080] Optimal swarm size

[0081] The swarm sensing system 2 aims at robust and accurate quantification, where the random noise due to a variety of sources discussed previously can be minimized by compiling readout from a large number of single nanoparticles 14 in the swarm of nanoparticles 14 (i.e., large swarm size). Statistically, a large sample size leads to a tighter confidence interval, indicating a greater precision in the final measurement output. This approach, however, may not always be practical due to increased instrumentation complexity and labor needed for repeated measurements. The swarm sensing scheme provides the flexibility to significantly increase sample size by imaging multiple single nanoparticle 14 sensors as independent measurements without increasing instrumentation complexity or prolonging detection time. The standard error of hue shift decreases as the swarm size increases, which converged at around 2,000 (FIG. 13). Therefore, a swarm size of about

2,000 single nanoparticles 14 achieves a good trade-off between high fidelity and measurement complexity, beyond which, the standard error, which indicates the accuracy of sample mean compared to the population mean, would not be significantly improved with increased swarm size.

[0082] Wide dynamic range using single nanoparticle swarms

[0083] As explained herein, nanoparticles 14 with 100 nm and 10 nm diameters achieve quantitative analog delta hue readout for individual nanoparticles 14 with random error minimized by assessing the majority "votes". For nanoplasmonic sensing, the swarm sensor system 2 provides significant advantages over "digital" assays, which evaluates individual sensing events with binary "on" and "off" output, in terms of dynamic range, operational concentrations and sensing accuracy. While other digital nanoplasmonic assays employing dimer particle structures (80nm and 40nm respectively) achieved a low limit of detection, the digital nature of the assay significantly limited the dynamic range of the assay. See e.g., Ungureanu et al., Immunosensing by colorimetric darkfield microscopy of individual gold nanoparticle-conjugates, Sensor Actuat B-Chem 150(2), 529-536 (2010) and Verdoold et al., Femtomolar DNA detection by parallel colorimetric darkfield microscopy of functionalized gold nanoparticles, Biosens Bioelectron 27(1), 77-81 (2011). With limited binding sites available on the surface of a single 80nm-AuNP for 40nm-AuNPs detector probes, only qualitative binary readout was achieved for individual AuNPs, and collectively one quantitative readout was generated per device representing the fraction of AuNPs with a positive color change, i.e., R/G ratio. As a result, this system exhibited a narrow dynamic range (2 orders of magnitude) in buffer solution and approached saturation at ultra-low concentrations (sub-picomolar). The swarm sensor system 2 instead considers each nanoparticle 14 as a separate analog sensor and accumulates the many quantitative readouts from a plurality of nanoparticles 14 to accumulate a more accurate final quantitative signal.

[0084] In addition, the presented swarm sensor system 2 overcomes the problem of low dynamic range by utilizing much smaller detector gold nanoparticles 14 (10nm) paired with large capture gold nanoparticles 14 (100nm) and demonstrated that the hue change induced by the binding of 10 nm nanoparticles 14 on a single 100-nm nanoparticle 14 can be quantitatively characterized over a range of concentrations; thereby achieving a quantitative analog signal per sensor nanoparticle 14. Experimental data indicated an average hue shift from 4 to 16 degrees was observed for each individual capture nanoparticle bound with a noise level around 2-3 degrees (FIG. 10B, 10D). This agrees well with FDTD simulation results that a maximum number of ~ 100 10nm-AuNPs could bind to the surface of a single

100 nm nanoparticle, inducing hue shifts ranging from 2 to 14 degrees (FIG. 7). Analysis of the histogram of a swarm of thousands (≥2000) gold nanoparticles 14 further improved the detection resolution by reducing the uncertainty of the delta hue to ~0.1, as indicated by the standard error of the swarm (FIGS. 10B, 10D). Therefore, a much wider dynamic range (4-6 logs) was achieved for protein detection using swarm sensing.

[0085] Improved sensing accuracy using individual hue shifts

[0086] For an ideal sensing device, where all the single nanoparticles 14 possess identical initial states and are predicted to perform in the same manner, only one set of dark field images would be necessary, after all of the reaction steps. In reality, the hue of individual nanoparticles 14 in the same FOV varies slightly (as seen in the "before" image in FIG. 3), leading to systematic error that is unique for each sensor. Compared to the analytical results using delta hue (FIGS. 10A-10D and 11A, 11B), results only using after-hue failed to establish a consistent trend with the increase of target analyte concentrations in buffer solutions (FIGS. 14A and 14B); and failed to differentiate among the three clinical ranges with statistical significance for detection in serum (FIGS. 15A, 15B), jeopardizing the confidence when interpreting sensor readouts. Many factors could contribute to the hue variations of single nanoparticle 14 sensors before detection, such as size distribution due to the fabrication process of bare particles (e.g., the hue histogram of bare particles, as shown in FIG. 9B) and conjugation efficiencies (e.g., the before-hue histogram of capture AuNPs conjugated with BSA/Anti-CRP, as shown in FIGS. 16A-16C).

[0087] In addition, dark field images only illustrate the scattered light from nanoparticles 14, which is typically larger than the actual particle size, therefore, the region of a single ROI does not represent the exact shape of an individual nanoparticle 14. During image analysis, parameters such as circularity and area of the ROI have been used as filters to facilitate the selection of single nanoparticles 14, however it is still possible that a circular ROI was in fact an aggregate of multiple nanoparticles 14. Accurate detection readout could also be affected by either the particle variation caused by conjugation, or the inconsistency of initial states of sensor chips (i.e., optically transparent substrates 12) during immobilization or imaging conditions. Overall, swarm sensing based on delta hue led to readout that was more tolerable to both individual particle variations (FIGS. 10A-10D), and device variation (FIGS. 11A and 11B).

[0088] High tolerance to non-specific binding for sensing in complex biofluids

[0089] Biosensing in biofluids remains challenging, as sensor performance is typically hindered by issues such as non-specific binding and sample variation, which is largely due to

the complex nature and matrix effect of the biofluids. Furthermore, biomarker detection becomes even more difficult when the clinical cutoffs are within a close range (e.g., < 10-fold). For example, the clinically relevant concentrations of CRP as a cardiac marker are at relatively high concentrations (i.e., μg/ml) with only around 3 times concentration differences separating different clinical classifications. The approach of using swarm sensing of nanoparticles 14 based on delta hue appears to be less sensitive to the non-specific binding on the device surface (FIG. 12), i.e., false positive signal was minimized. One potential reason is that since ROIs were pre-defined by the "before" image, only signals from the areas corresponding to nanoparticle 14 "sensors" were analyzed. In addition, the detector nanoparticles 14 (AuNPs with 10 nm diameter) do not generate interfering signal alone because the exposure time used during dark field imaging was too low for these smaller nanoparticles 14 to generate sufficient scattered light alone. On the other hand, despite the interference of matrix effects exerted on the assay performance, i.e., lower signal (FIGS. 16B, 16C), the system 2 described herein avoids sources of systematic and random errors introduced by sample matrices, and differentiates clinical cutoffs with < 10 fold difference in concentration with robust readouts, demonstrating significant potential for biosensing in clinical settings.

[0090] Informative sensing by examining pre-hue vs. delta-hue

[0091] Because the status of each single nanoparticle 14 before and after sensing were both recorded, the detection results of each single nanoparticle 14 can be mapped versus its initial state, which provides further "quality control" capabilities to identify optimal/reliable nanoparticle 14 in the swarm. The scatter plot of each device with thousands of single nanoparticle 14 sensors typically shows a triangular shape (FIGS. 17A-17C). The distribution of before-hue on the x-axis represents the sensor variation due to particle size and conjugation using different protein markers, e.g., BSA and anti-CRP (FIGS. 16A, 16B). As shown in the before-hue histogram in FIGS., 16A-16C, the majority of the nanoparticle 14 population initially exhibited a hue around 80°. It is hypothesized that the region in between 70° to 90° represents typical 100nm diameter single nanoparticles 14 with a complete conjugation layer. Higher before-hue (> 90°), which is very rare, could indicate outliers with incomplete conjugation. Lower before-hue regions (< 60°) may be associated with non-specific binding to the nanoparticle 14 surface during immobilization and potential particle aggregates. The range of the distribution along the y-axis (after-hue) for each before-hue region varies, which could be to the result of different numbers of chemical species 4 and detector nanoparticles 14 bound to a single capture nanoparticle 14. The largest distribution

of delta hue was typically around a before-hue near 80°, where the sensors were well-dispersed single nanoparticles 14 fully conjugated to allow for the maximum number of binding sites available. Sensors exhibiting higher before-hues may generate a reduced hue shift because of less binding sites available after incomplete conjugation. The maximum delta hue (~ 40°) is achieved when a capture nanoparticle 14 has the maximum number of binding sites all saturated by detector nanoparticles 14. Therefore, the distribution of delta hue at the lower before-hue region (< 60°) is limited to a smaller range, as indicated by the slope in the scatter plot. When detection occurred in serum, the maximum delta hue on the y-axis was significantly lower with a much tighter distribution compared to that in buffer solution (FIGS. 16B, 16C), possibly due to matrix effects in serum where some of the target antigen 4 interacts with matrix components in serum instead of forming target antigen-antibody pairs. This informative sensing capability allows the evaluation of the sensor status for quality control, provides useful information for troubleshooting, and potentially enables protein marker dependent optimization.

[0092] Reduced instrument complexity for point-of-care applications

[0093] To minimize variations due to random noise and the inconsistency of the devices, either multiple measurements from the same device (e.g., LSPR biosensors equipped with spectrometers) or multiple measurements from different locations or wells (e.g., ELISA, PCR) are performed. Such an approach to make multiple measurements is limited by the cost, time, reagent usage, and instrument complexity for each sensing device. On the contrary, the swarm sensing approach described herein uses single nanoparticle colorimetry treats well-dispersed single nanoparticles 14 as individual sensors that each get a vote as part of a swarm of parallel reactions. In addition, signal collection using dark field imaging instead of spectral shift measurements with spectrometers provides easy access to the location information of each nanoparticle 14, i.e., the swarm sensor. The combination of these two elements led to a low-cost solution for the simultaneous detection of hundreds of single nanoparticle 14 sensors located in one FOV, and normalization to an initial condition to avoid systematic error, which significantly increased the confidence in a measured result.

[0094] A nanoplasmonic biosensing system 2 is thus disclosed that is based on massively parallel analyses of a swarm of single nanoparticle 14 colorimetric sensors, which provides informative sensing by evaluating sensor status both before and after sensing. This sensing scheme provides an alternative to conventional ensemble-based LSPR detection approaches. With instrumentation that can be simple and cost effective, it has the potential to be implemented as a handheld point-of-care device. Rapid readouts from thousands of single

nanoparticle 14 sensors combined with individual evaluation using delta hue renders higher tolerance for particle variations, device variations, and sample variability. With minimized interference from non-specific binding in the background, the successful detection of clinical cutoffs within a close range of concentrations was possible in complex biofluids without the need of blocking steps. In addition, the simplicity of the sensor chip and particle preparation in colloidal solution without the need of nanofabrication significantly lowered the assay cost and make it a promising candidate for point-of-care readers using consumer electronics to perform dark-field imaging and multiplexed sensing. Furthermore, the methodology of swarm sensing is versatile. Its application is not limited to nanoplasmonic platforms, and could be adapted by other types of single entity-based sensors, such as fluorescence, electrochemical, and magnetic for robust detection with statistically improved accuracy and reproducibility, as long as high-throughput readout from a large pool of individual sensors can be conducted efficiently using either imaging or other parallelized analysis methods.

[0095] While embodiments of the present invention have been shown and described, various modifications may be made without departing from the scope of the present invention. The invention, therefore, should not be limited, except to the following claims, and their equivalents.

What is claimed is:

1. A system for determining the presence and/or concentration of an analyte in a sample comprising:

an optically transparent substrate having a plurality of plasmonic nanoparticles immobilized on a surface thereof;

a dark field imaging device configured to acquire color images of the optically transparent substrate before and after exposure to the analyte;

image processing software configured to define regions of interest (ROIs) in the acquired color images, the ROIs representing individual plasmonic nanoparticles, wherein the image processing software is further configured to extract color intensity values from one or more color channels from each ROI to calculate a hue value for individual plasmonic particles before and after exposure to the analyte, wherein the image processing software calculates a delta hue value from the respective before and after hue values for the individual plasmonic nanoparticles and wherein the presence and/or concentration of the analyte is based on the delta hue values of the plasmonic nanoparticles.

2. The system of claim 1, wherein the plasmonic nanoparticles comprise gold or silver plasmonic nanoparticles.

3. The system of claims 1 or 2, wherein the plasmonic nanoparticles comprise first capture plasmonic nanoparticles bound to the analyte and second detector plasmonic nanoparticles bound to the analyte.

4. The system of claim 3, wherein the second detector plasmonic nanoparticles comprise gold or silver plasmonic nanoparticles.

5. The system of claim 3, wherein the second detector plasmonic nanoparticles are smaller than the first capture plasmonic nanoparticles.

6. The system of claim 1, wherein the optically transparent substrate comprises a microfluidic channel, well, or reservoir located within a chip.

7. The system of claim 1, wherein the analyte comprises a protein, protein fragment, nucleic acid, microRNA, antibody, antigen, drug, biomolecule, virus, exosome/microvesicle, or drug metabolite.

8. The system of claim 1, wherein the plasmonic nanoparticles comprise capture nanoparticles having an antibody conjugated thereto.

9. The system of claim 8, wherein the plurality of plasmonic nanoparticles are conjugated to the same antibody.

10. The system of claim 8, wherein the plurality of plasmonic nanoparticles are conjugated to different antibodies.

11. The system of claim 8, wherein the plasmonic nanoparticles comprise nanoparticles of a first type and nanoparticles of a second type.

12. The system of claim 11, wherein the plasmonic nanoparticles of the first type are located on the optically transparent substrate in different spatial locations than the plasmonic nanoparticles of the second type.

13. The system of claim 11, wherein the plasmonic nanoparticles of the first type exhibit hue values that are different from hue values exhibited by the plasmonic nanoparticles of the second type prior to exposure to the analyte.

14. The system of claim 8, further comprising detector nanoparticles configured to bind to the location(s) where capture nanoparticles have bound analyte.

15. The system of claim 1, wherein the optically transparent substrate comprises one or more fiducial marks thereon.

16. The system of claim 8, wherein the capture nanoparticles are co-localized on the optically transparent substrate with a fluorophore.

17. A method for determining the presence and/or concentration of an analyte in a sample comprising:

providing an optically transparent substrate having a plurality of plasmonic nanoparticles immobilized on a surface thereof;

imaging the optically transparent substrate before the sample has been applied with a dark field imaging device configured to acquire one or more before color images of the optically transparent substrate;

loading the optically transparent substrate with the sample;

imaging the optically transparent substrate after the sample has been applied with a dark field imaging device configured to acquire one or more after color images of the optically transparent substrate;

subjecting the respective before and after color images to image processing software configured to define regions of interest (ROIs) in the respective before and after color images, the ROIs representing individual plasmonic nanoparticles, wherein the image processing software is further configured to extract color intensity values from one or more color channels from each ROI to calculate a hue value for individual plasmonic particles in the respective before and after color images, wherein the image processing software calculates a delta hue value from the respective before and after hue values for the individual plasmonic particles and wherein the presence and/or concentration of the analyte is based on the delta hue values of the plasmonic nanoparticles.

18. The method of claim 17, wherein the plasmonic nanoparticles comprise gold or silver plasmonic nanoparticles.

19. The method of claims 17 or 18, wherein the plasmonic nanoparticles comprise first capture plasmonic nanoparticles bound to the analyte and second detector plasmonic nanoparticles bound to the analyte.

20. The method of claim 19, wherein the second detector plasmonic nanoparticles comprise gold or silver plasmonic nanoparticles.

21. The method of claim 19, wherein the second detector plasmonic nanoparticles are smaller than the first capture plasmonic nanoparticles.

22. The method of claim 17, wherein the optically transparent substrate comprises a microfluidic channel, well, or reservoir located within a chip.

23. The method of claim 17, wherein the analyte comprises a protein, protein fragment, nucleic acid, microRNA, antibody, antigen, drug, biomolecule, virus, exosome/microvesicle, or drug metabolite.

24. A system for determining the presence and/or concentration of an antibody in a sample comprising:

an optically transparent substrate having a plurality of plasmonic nanoparticles immobilized on a surface thereof and conjugated to an analyte specific for the antibody;

a dark field imaging device configured to acquire color images of the optically transparent substrate before and after exposure to the antibody;

image processing software configured to define regions of interest (ROIs) in the acquired color images, the ROIs representing individual plasmonic nanoparticles, wherein the image processing software is further configured to extract color intensity values from one or more color channels from each ROI to calculate a hue value for individual plasmonic particles before and after exposure to the antibody, wherein the image processing software calculates a delta hue value from the respective before and after hue values for the individual plasmonic nanoparticles and wherein the presence and/or concentration of the antibody is based on the delta hue values of the plasmonic nanoparticles.

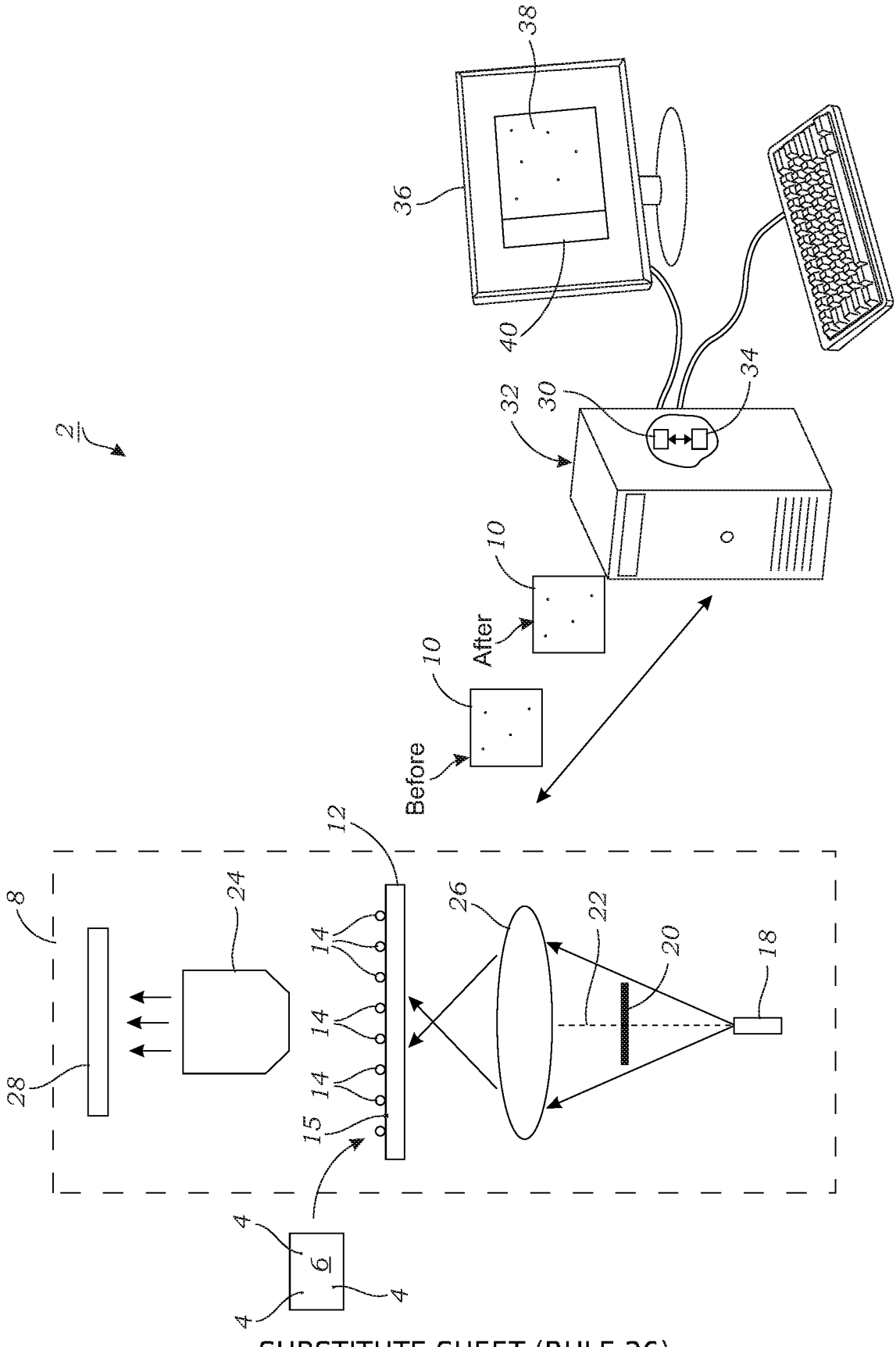
2
38
36
40
34
32
30
10
After
10
Before
12
8
24
26
22
20
18
14
14
14
15
28
4
6
4
4

FIG. 1

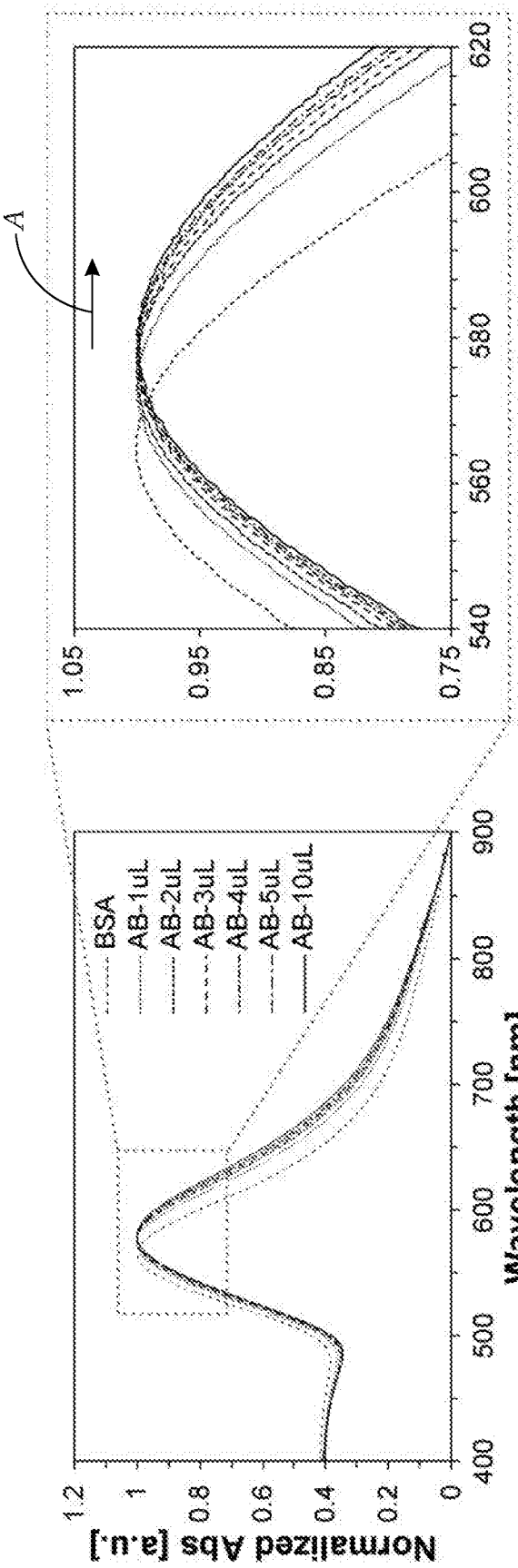
A
Normalized Abs [a.u.]
Wavelength [nm]
BSA
AB-1uL
AB-2uL
AB-3uL
AB-4uL
AB-5uL
AB-10uL

FIG. 2A

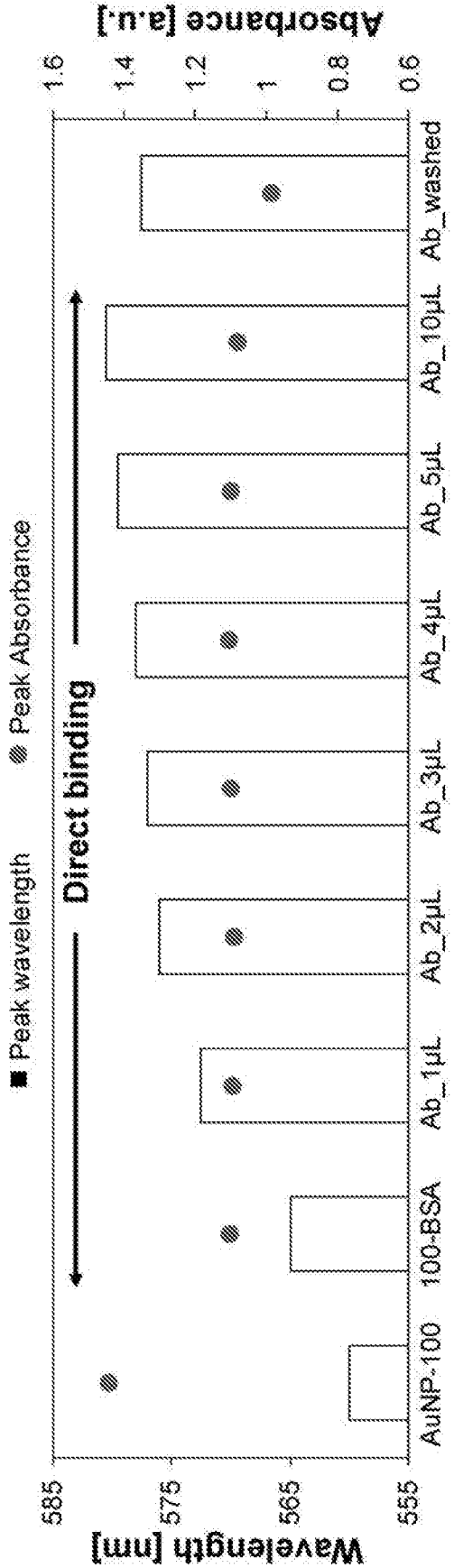
Absorbance [a.u.]
Wavelength [nm]
Peak wavelength
Peak Absorbance
Direct binding
AuNP-100
100-BSA
Ab_1µL
Ab_2µL
Ab_3µL
Ab_4µL
Ab_5µL
Ab_10µL
Ab_washed

FIG. 2B

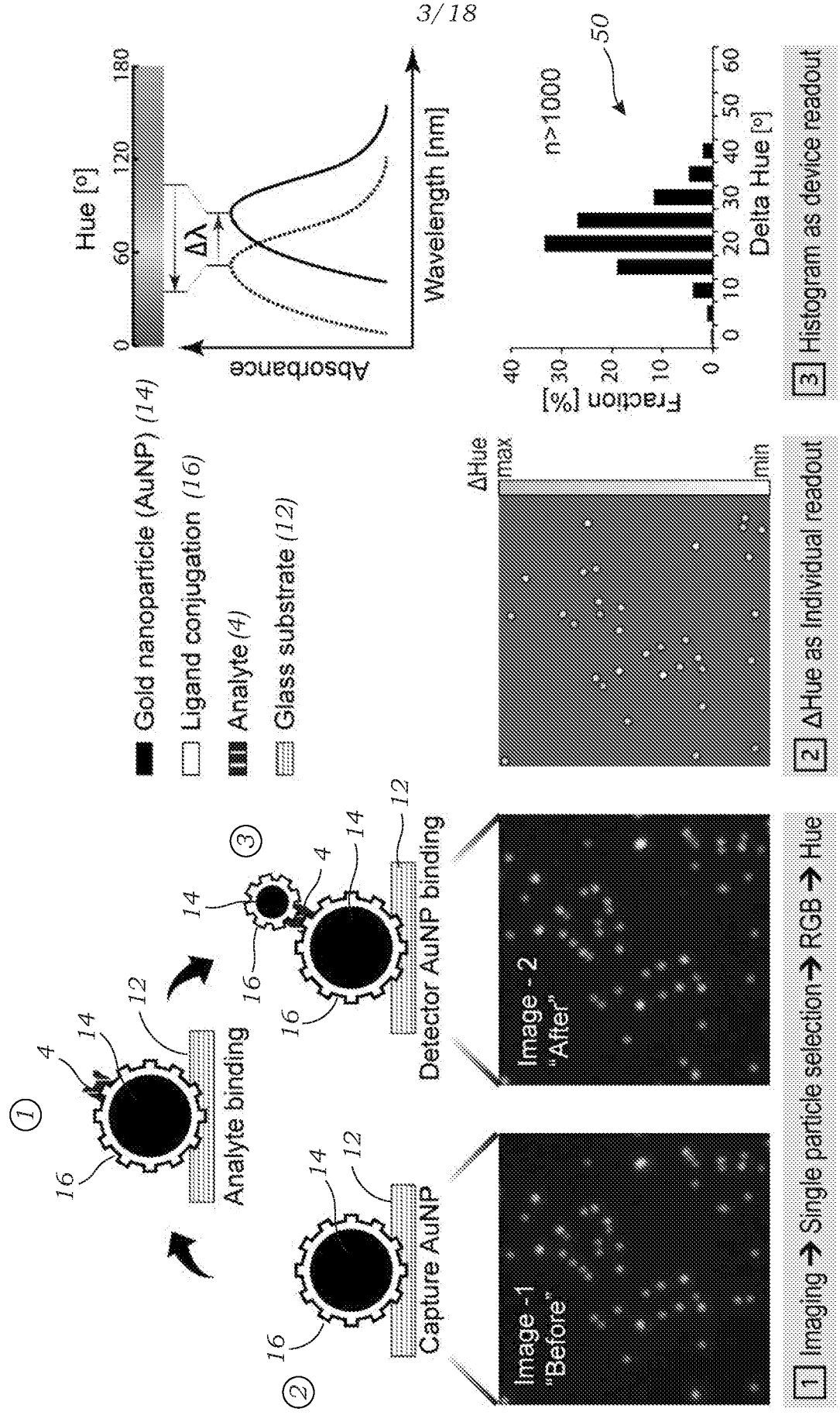
Gold nanoparticle (AuNP) (14)
Ligand conjugation (16)
Analyte (4)
Glass substrate (12)
Capture AuNP
Analyte binding
Detector AuNP binding
Image -1 "Before"
Image - 2 "After"
ΔHue
max
min
Hue [°]
Absorbance
Wavelength [nm]
Δλ
n>1000
Fraction [%]
Delta Hue [°]
1 Imaging → Single particle selection → RGB → Hue
2 ΔHue as Individual readout
3 Histogram as device readout

FIG. 3

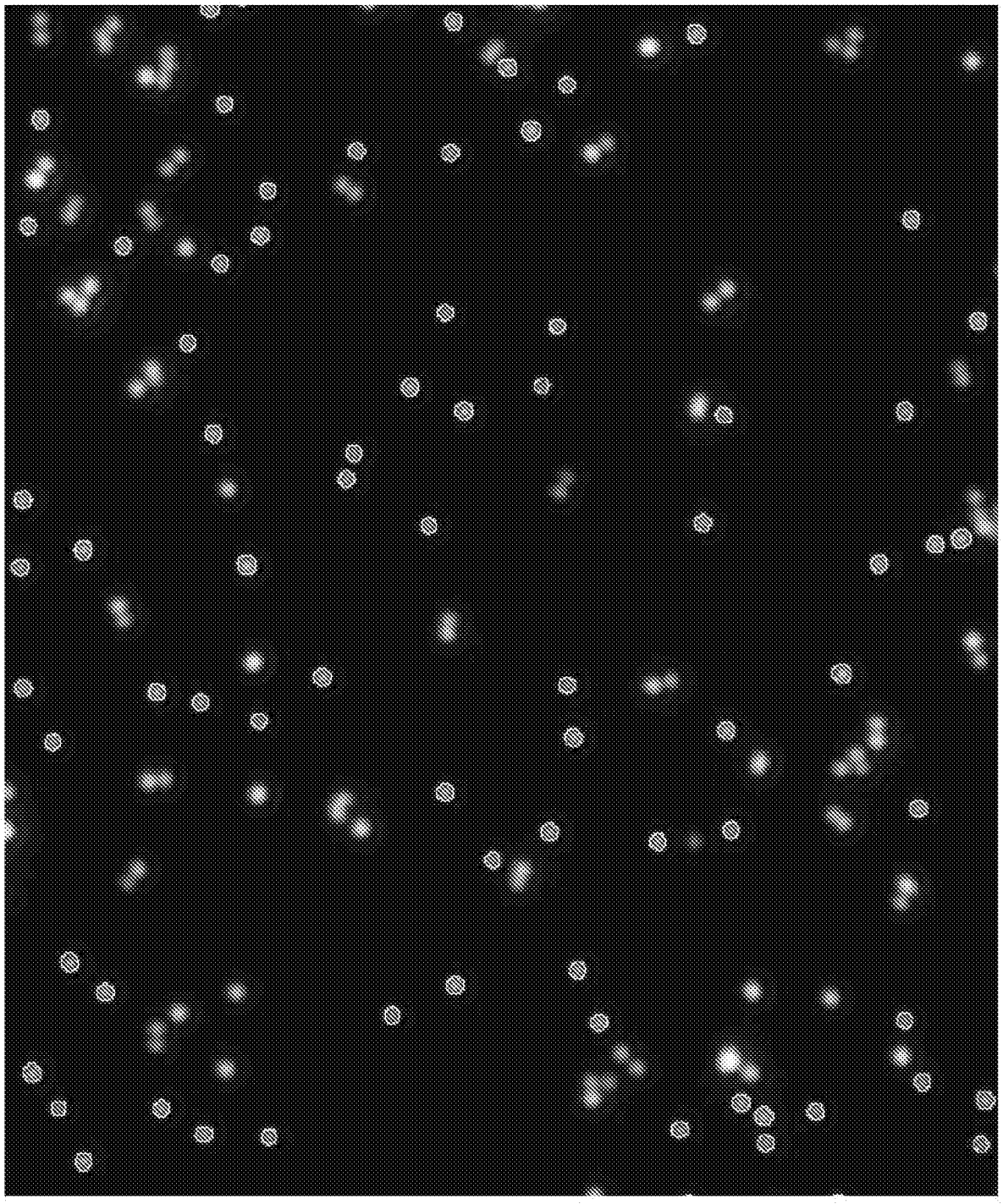

FIG. 4

Capture AuNP	20nm	60nm	100nm	150nm
Conjugation	✓	✓	✓	✓
Color change	×	×	✓	✓
Dark field imaging (DFM)	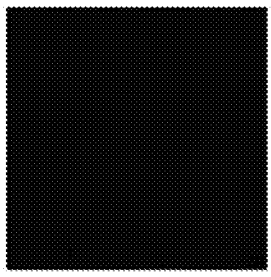	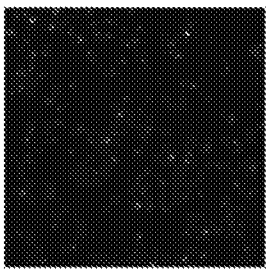	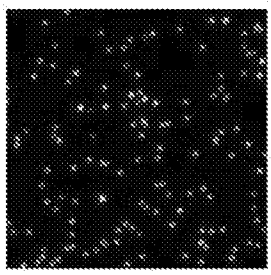	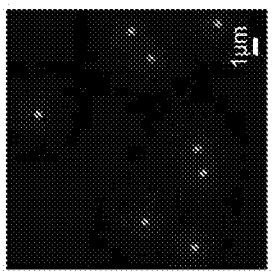

FIG. 5

Detector AuNP	4nm	10nm	20nm	60nm
Conjugation	×	✓	✓	✓
DFM background	✓	✓	✓	×
Sandwiched pair enhancement	×	✓	✓	×
SEM				

FIG. 6

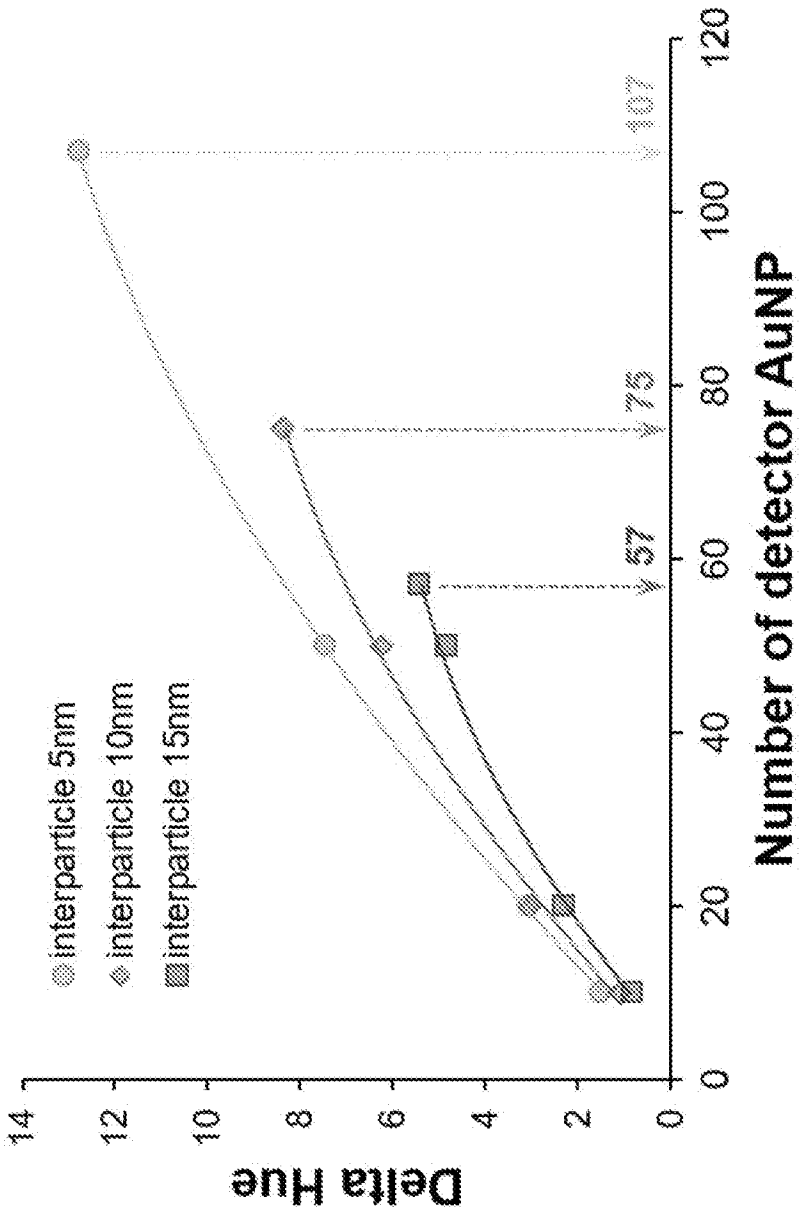
Delta Hue
Number of detector AuNP
interparticle 5nm
interparticle 10nm
interparticle 15nm
107
75
57
0
2
4
6
8
10
12
14
0
20
40
60
80
100
120

FIG. 7

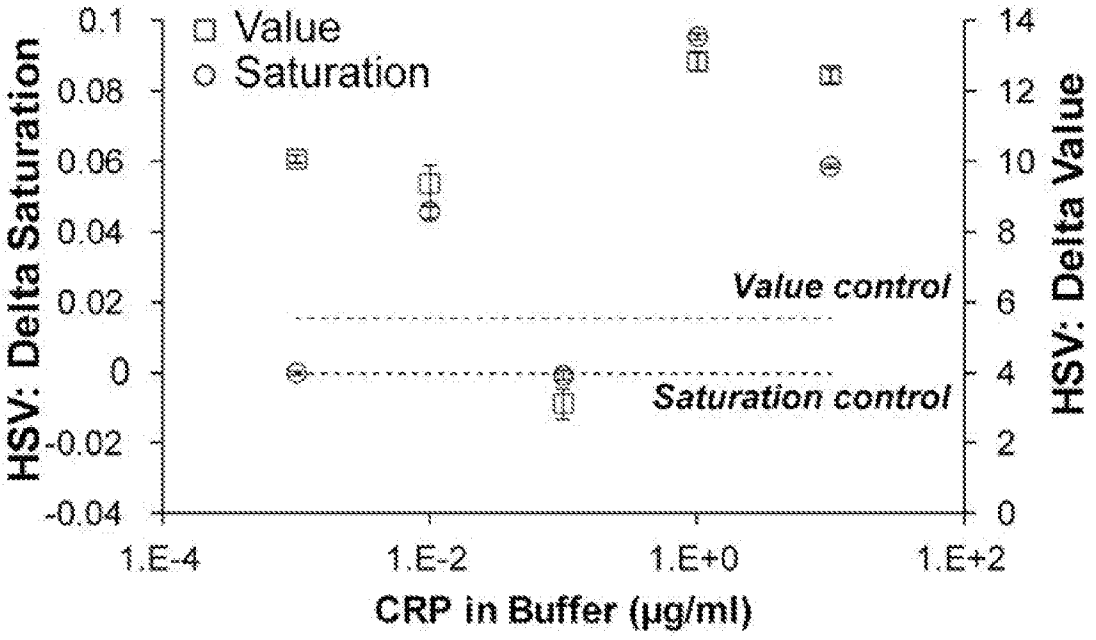
Value
Saturation
HSV: Delta Saturation
HSV: Delta Value
0.1
0.08
0.06
0.04
0.02
0
-0.02
-0.04
14
12
10
8
6
4
2
0
Value control
Saturation control
1.E-4
1.E-2
1.E+0
1.E+2
CRP in Buffer (µg/ml)

FIG. 8A

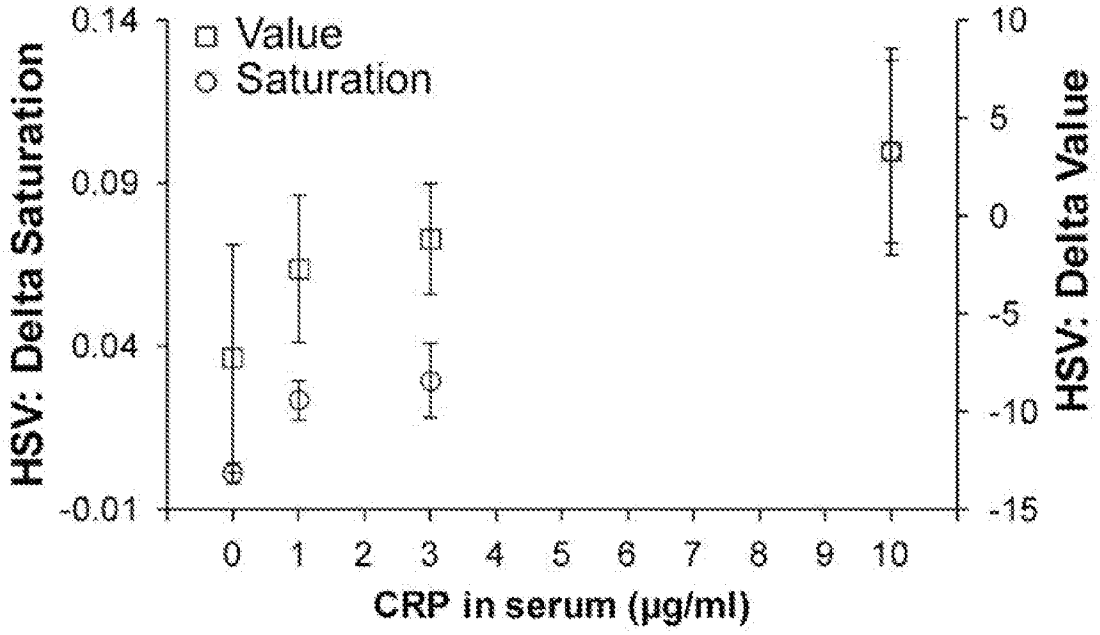
Value
Saturation
HSV: Delta Saturation
HSV: Delta Value
0.14
0.09
0.04
-0.01
10
5
0
-5
-10
-15
0
1
2
3
4
5
6
7
8
9
10
CRP in serum (µg/ml)

FIG. 8B

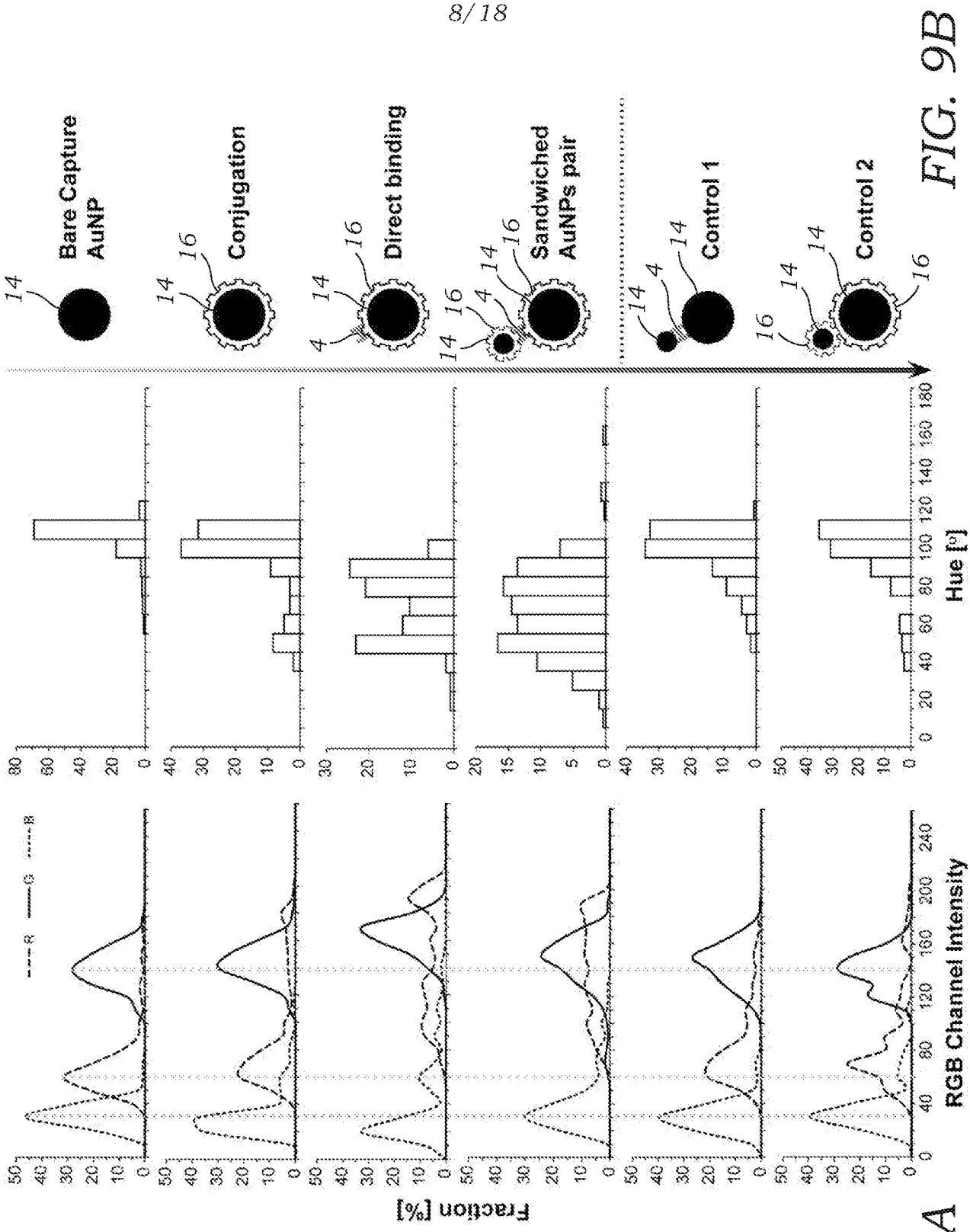
Bare Capture AuNP
Conjugation
Direct binding
Sandwiched AuNPs pair
Control 1
Control 2
Hue [°]
RGB Channel Intensity
Fraction [%]

FIG. 9A

FIG. 9B

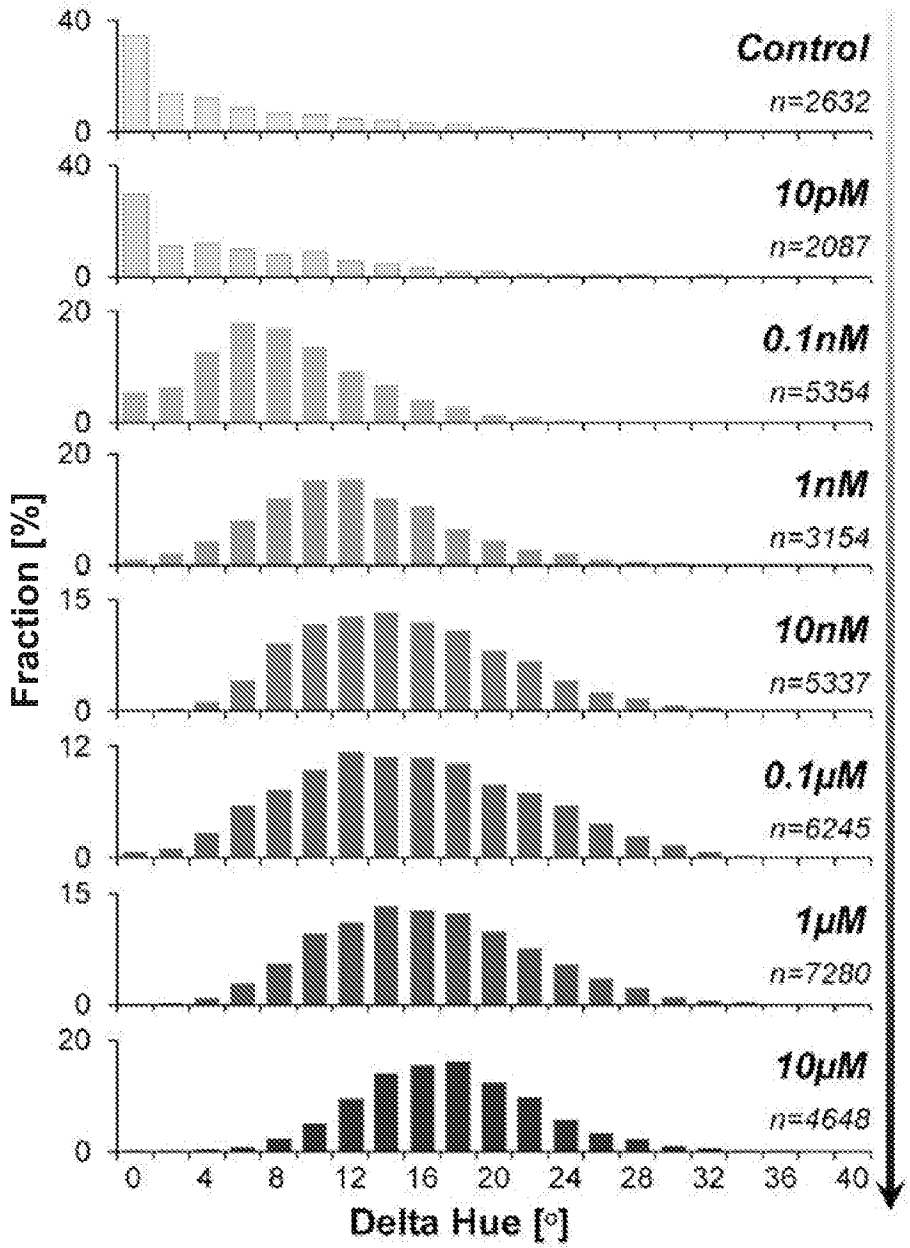

FIG. 10A

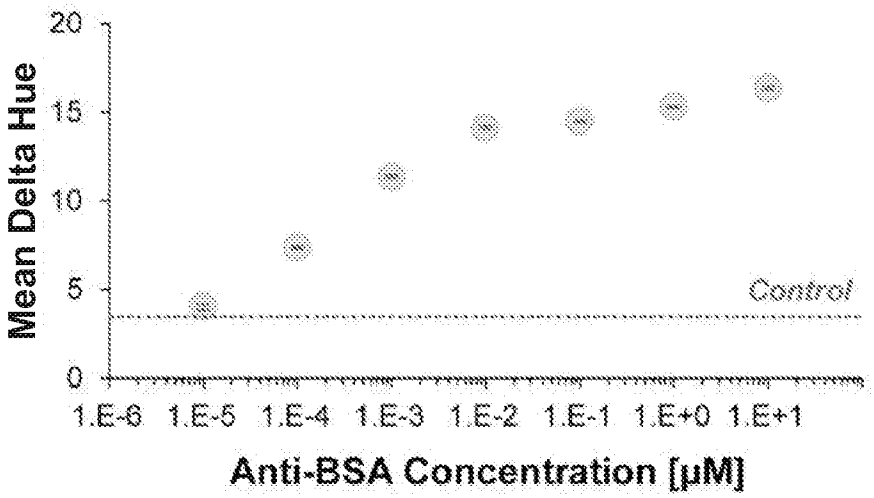

FIG. 10B

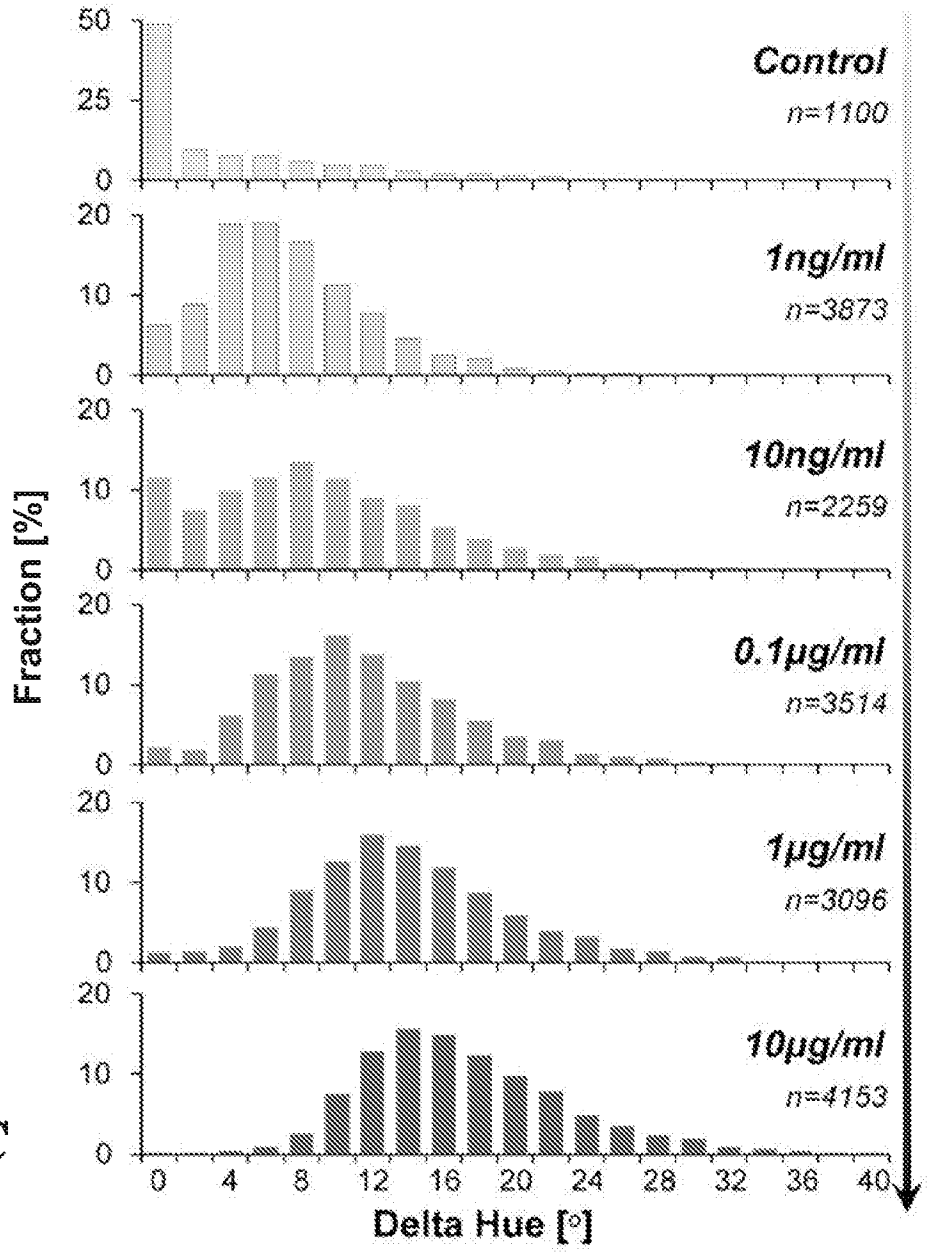

FIG. 10C

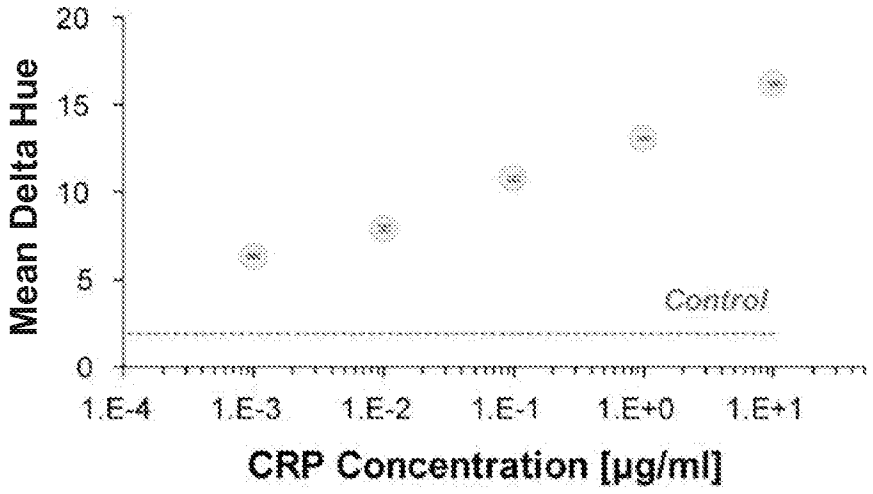

FIG. 10D

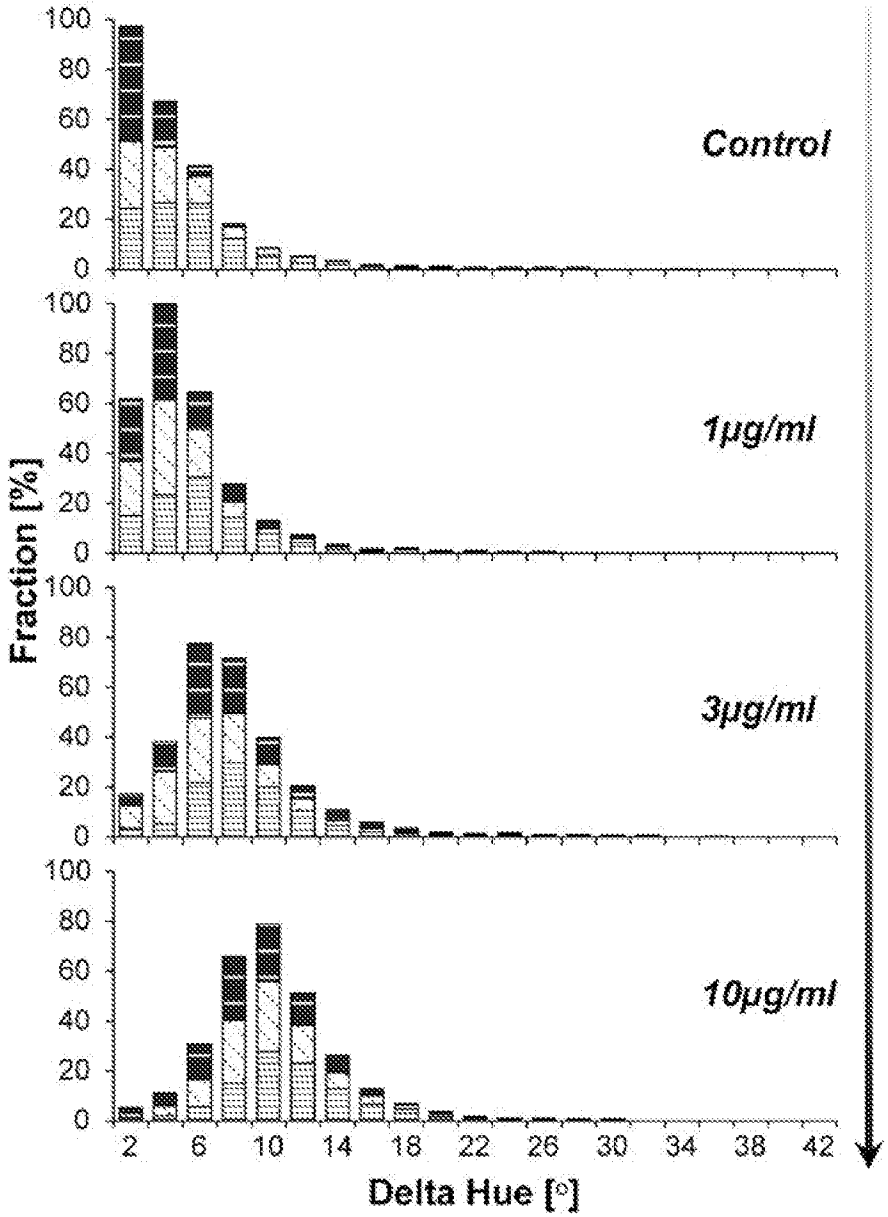

FIG. 11A

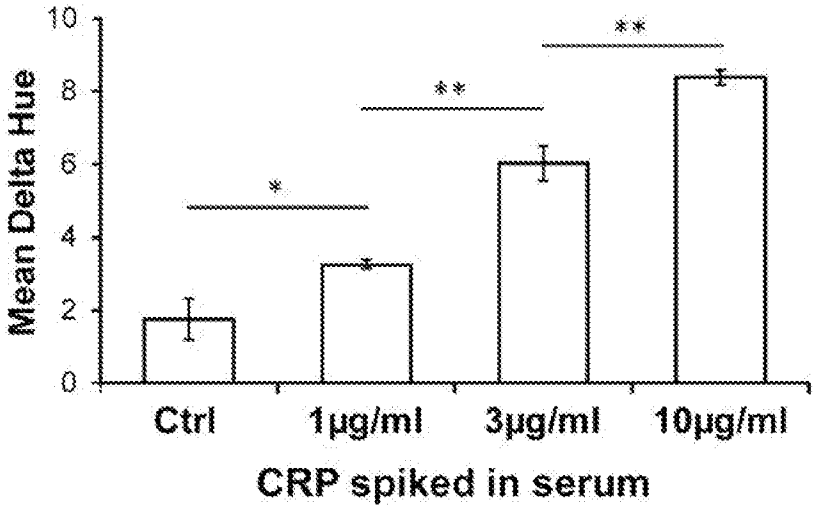

FIG. 11B

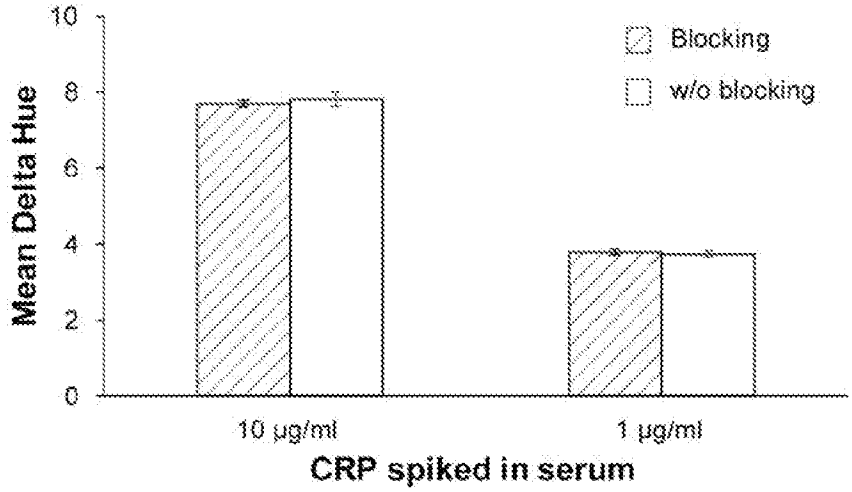
Mean Delta Hue
10
8
6
4
2
0
Blocking
w/o blocking
10 µg/ml
1 µg/ml
CRP spiked in serum

FIG. 12

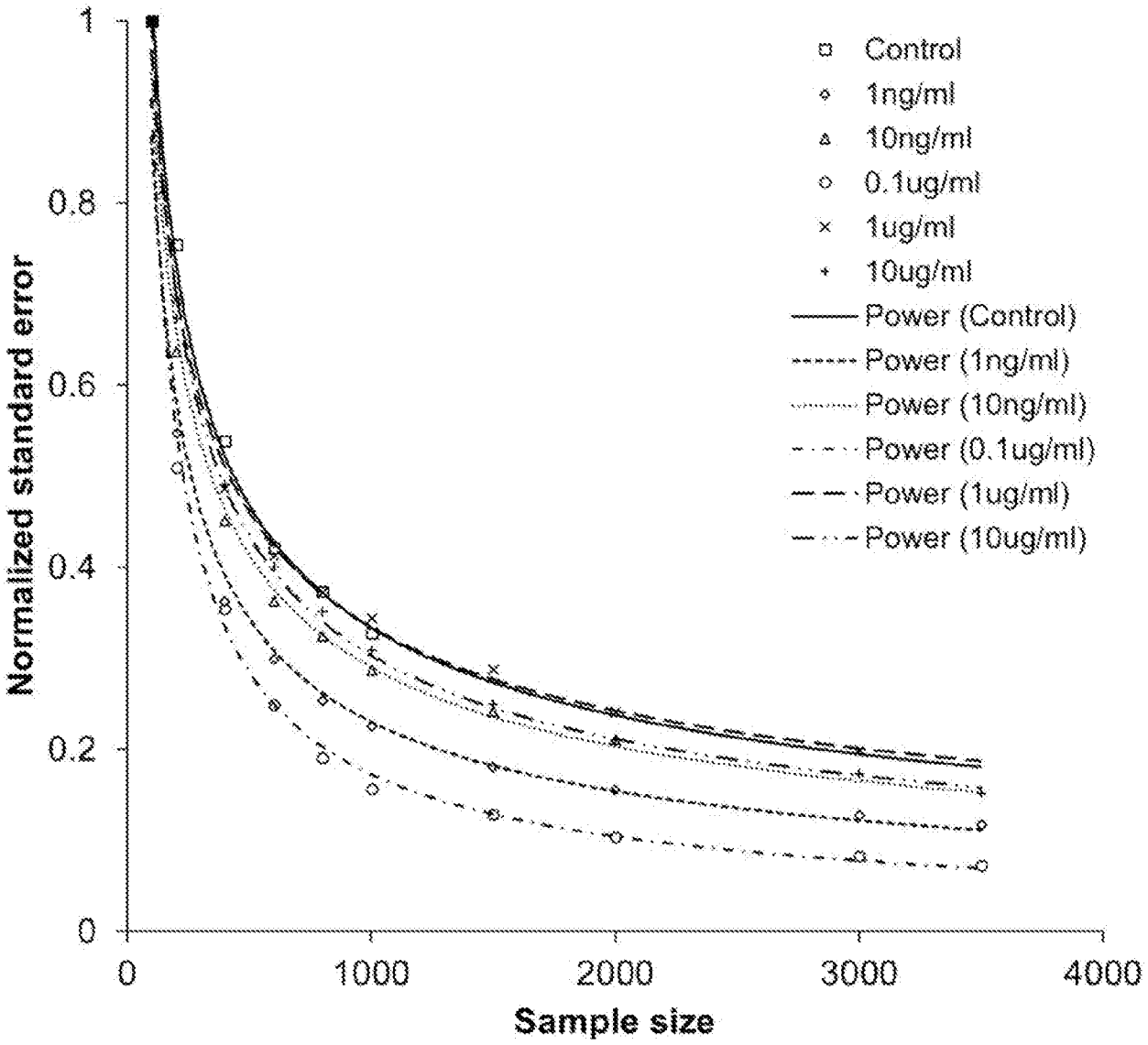
Normalized standard error
1
0.8
0.6
0.4
0.2
0
0
1000
2000
3000
4000
Sample size
Control
1ng/ml
10ng/ml
0.1ug/ml
1ug/ml
10ug/ml
Power (Control)
Power (1ng/ml)
Power (10ng/ml)
Power (0.1ug/ml)
Power (1ug/ml)
Power (10ug/ml)

FIG. 13

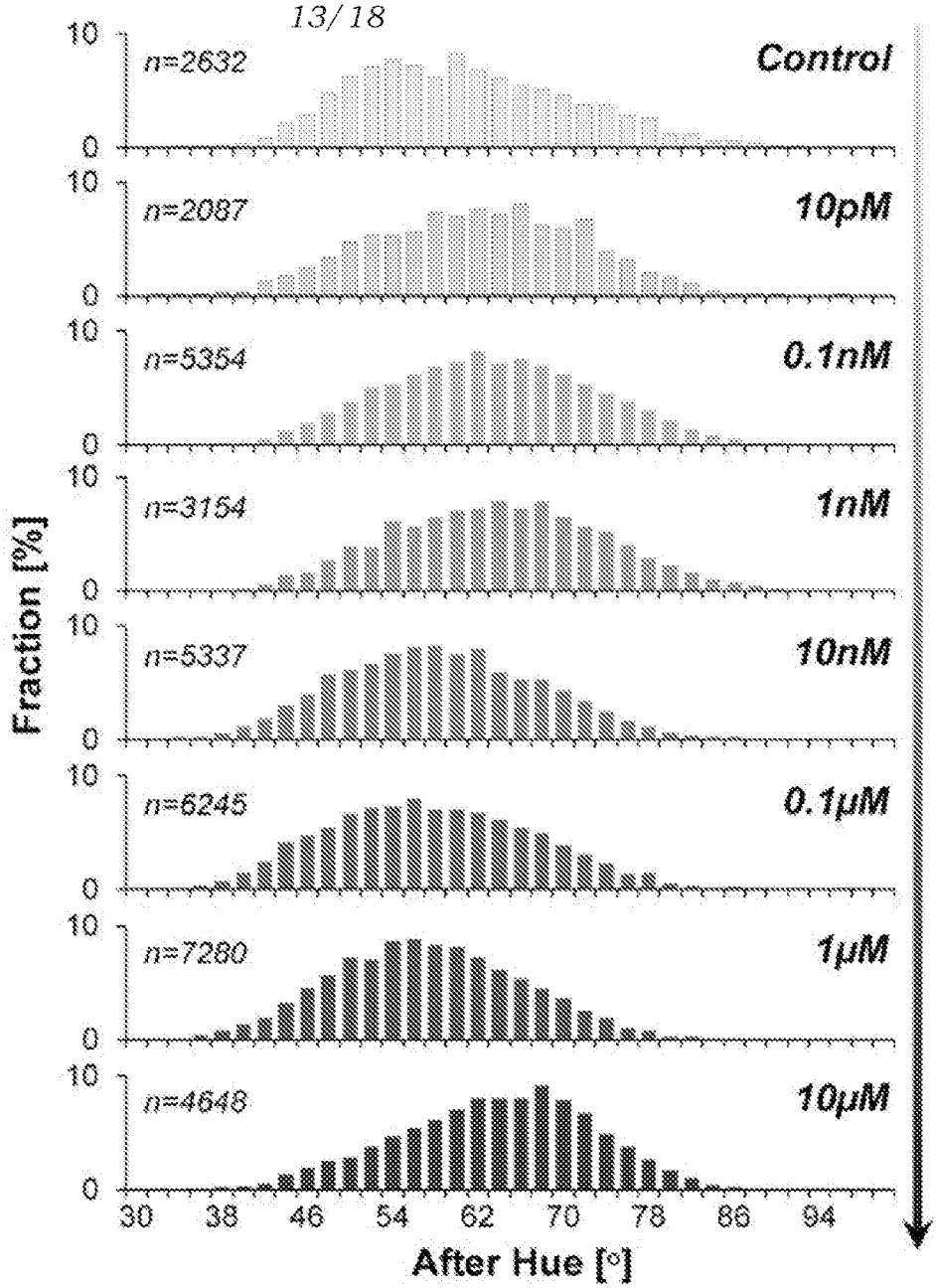

FIG. 14A

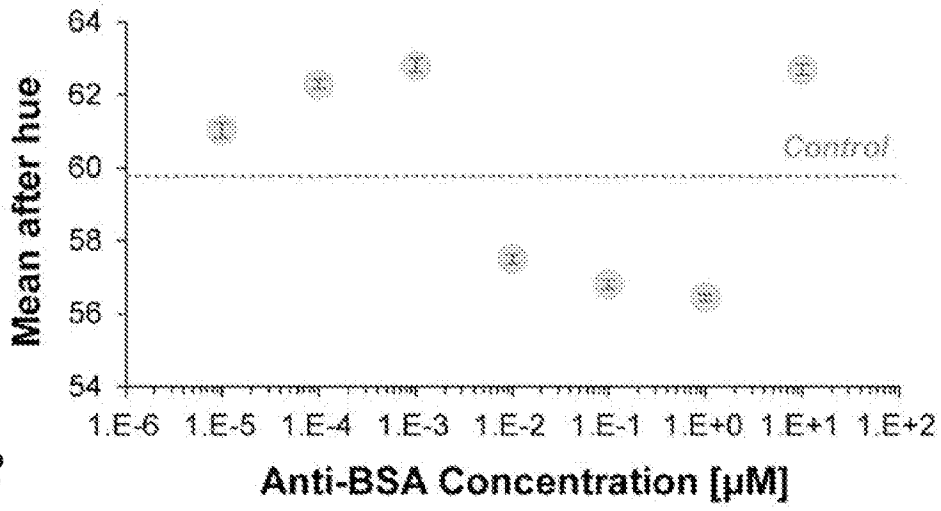

FIG. 14B

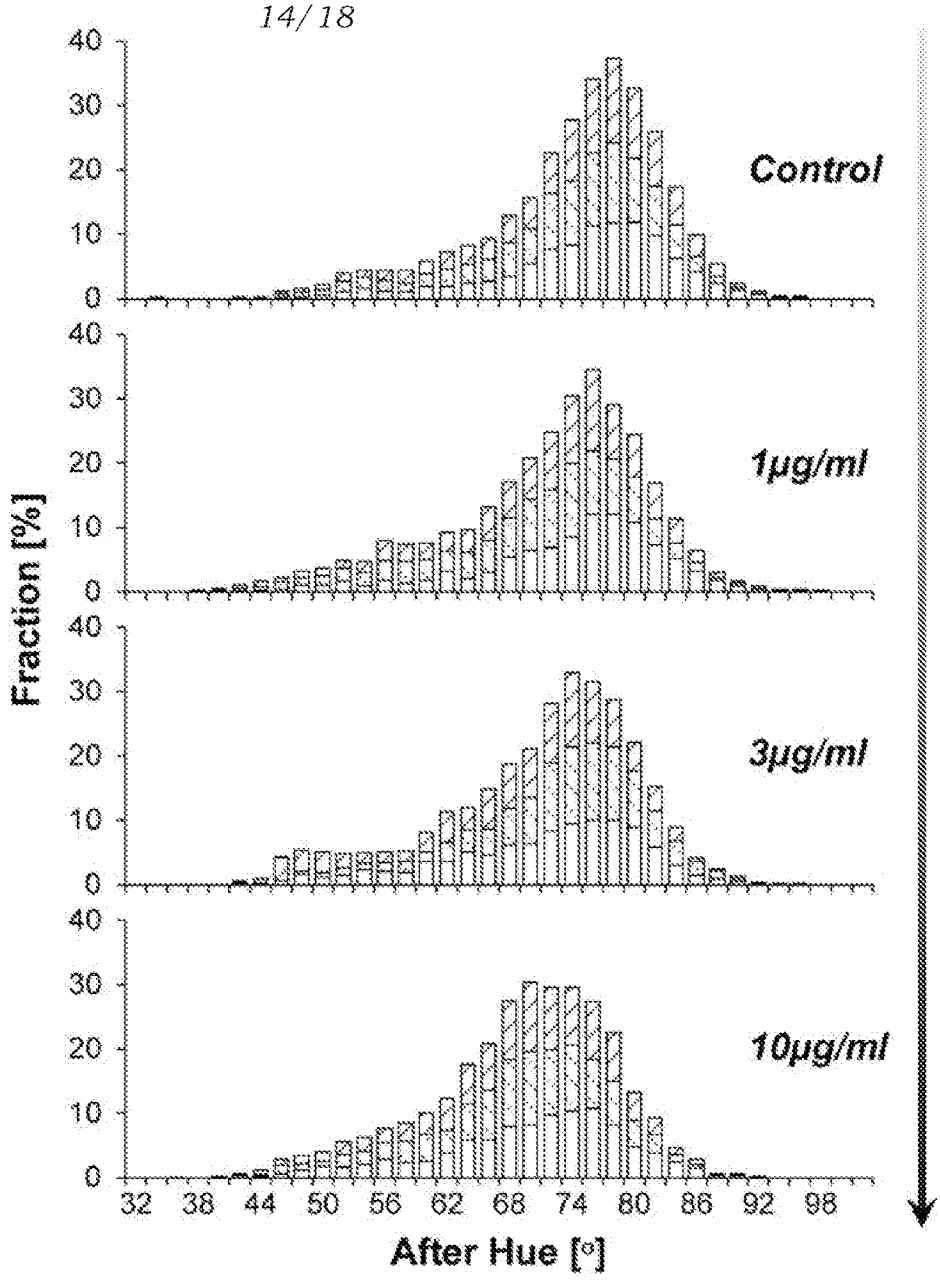

FIG. 15A

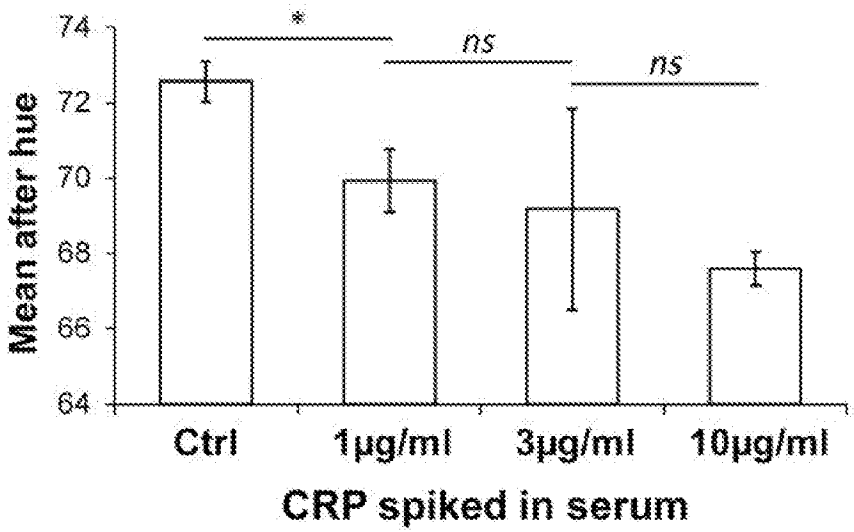

FIG. 15B

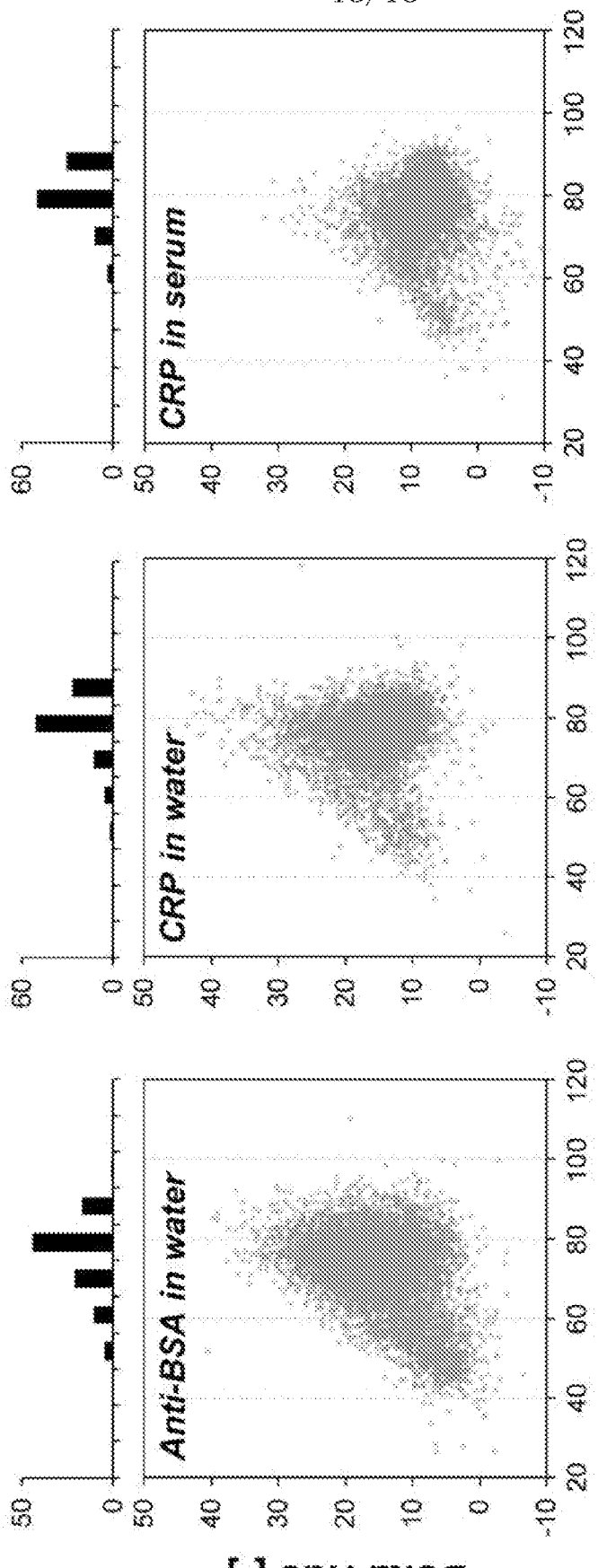

FIG. 16A

FIG. 16B

FIG. 16C

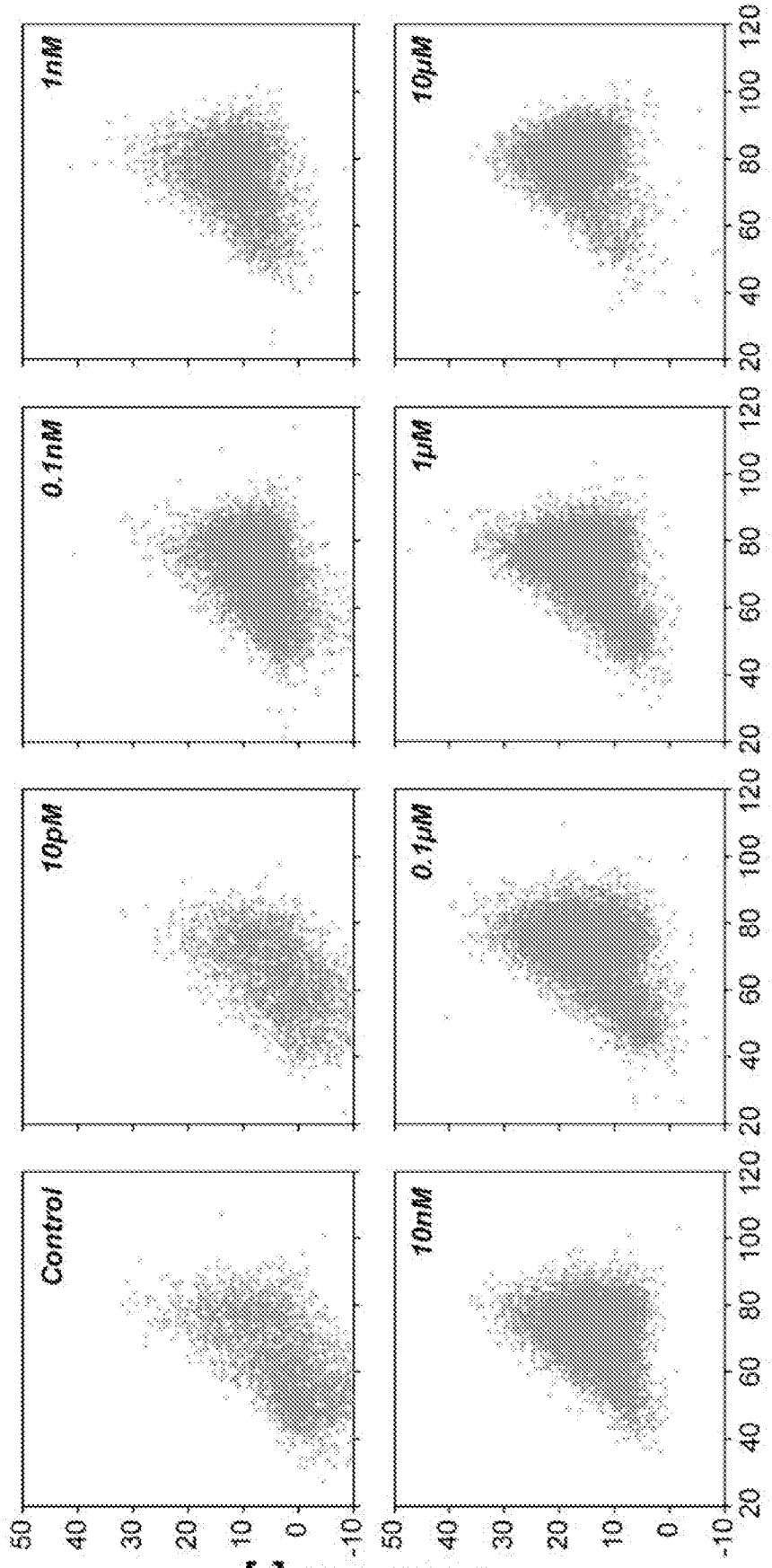
Control
10pM
0.1nM
1nM
10nM
0.1μM
1μM
10μM
Delta Hue [°]
Before Hue [°]
50
40
30
20
10
0
-10
20
40
60
80
100
120

FIG. 17A

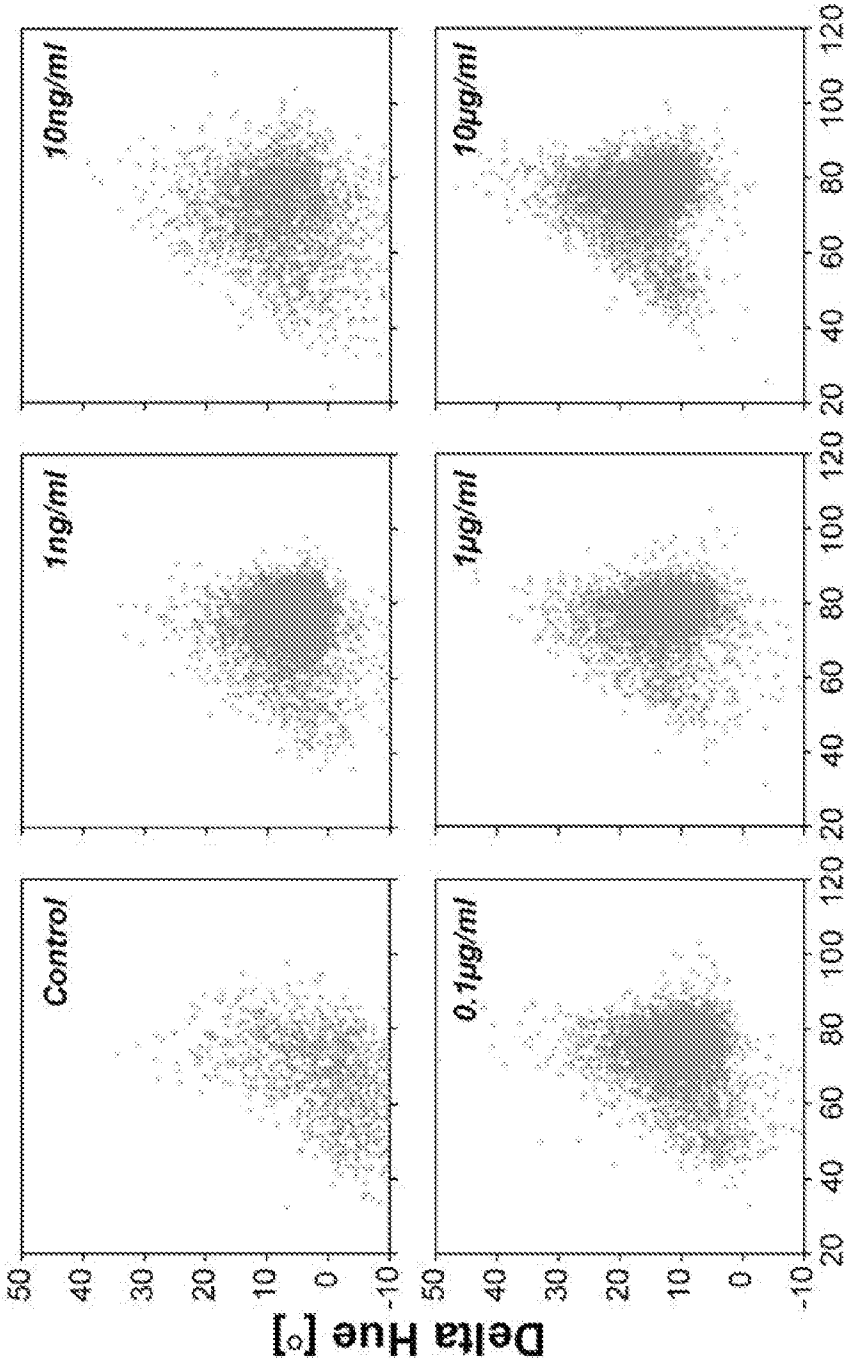
Control
1ng/ml
10ng/ml
0.1µg/ml
1µg/ml
10µg/ml
Delta Hue [°]
Before Hue [°]
50
40
30
20
10
0
-10
20
40
60
80
100
120

FIG. 17B

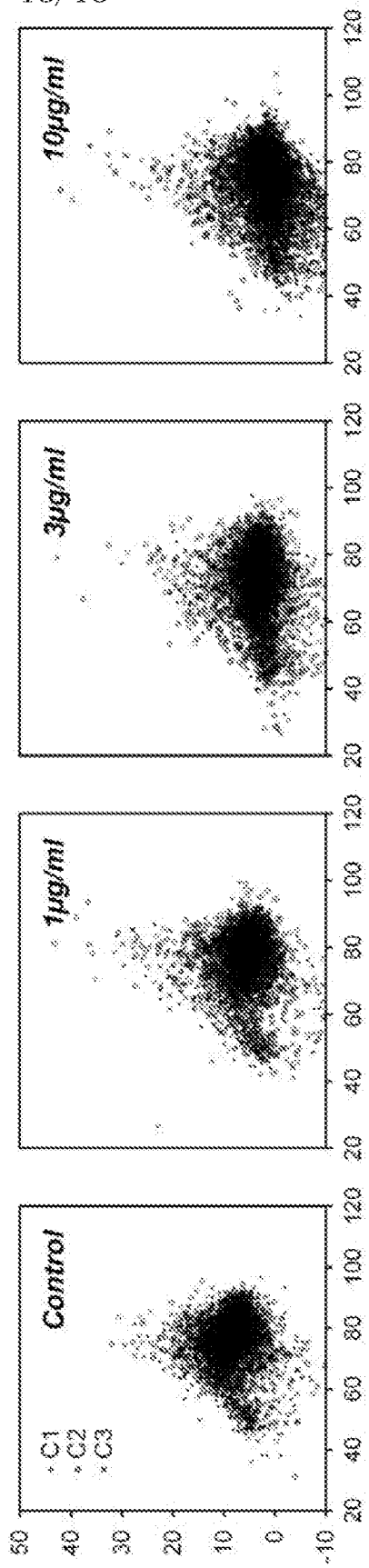

FIG. 17C

INTERNATIONAL SEARCH REPORT

International application No.
PCT/US19/38539

A. CLASSIFICATION OF SUBJECT MATTER

IPC - B82Y 15/00; G01N 33/50, 33/543 (2019.01)

CPC - B82Y 15/00; G01N 21/648, 33/50, 33/543, 33/54346

According to International Patent Classification (IPC) or to both national classification and IPC

B. FIELDS SEARCHED

Minimum documentation searched (classification system followed by classification symbols)
See Search History document

Documentation searched other than minimum documentation to the extent that such documents are included in the fields searched
See Search History document

Electronic data base consulted during the international search (name of data base and, where practicable, search terms used)
See Search History document

C. DOCUMENTS CONSIDERED TO BE RELEVANT

Category*	Citation of document, with indication, where appropriate, of the relevant passages	Relevant to claim No.
X --- Y	WO 2015/130980 A1 (LAMDAGEN CORPORATION) 03 September 2015; paragraphs [0050], [0054], [0064]-[0066]	1-14, 17-24 --- 15, 16
Y	NANOCOMPOSIX "Gold Nanoparticles: Optical Properties" [online article] 10 July 2017. [retrieved online: 20 August 2019] Retrieved from: <URL: https://nanocomposix.com/pages/gold-nanoparticles-optical-properties>; page 1, last paragraph	5, 21
Y	US 8,333,932 B2 (LEE, K et al.) 18 December 2012; column 4, line 57 to column 5, line 18; column 6, line 48	15
Y	US 2012/0208174 A1 (GALUSH, W et al.) 16 August 2012; paragraphs [0097]-[0098]	16

☐ Further documents are listed in the continuation of Box C. ☐ See patent family annex.

* Special categories of cited documents:
"A" document defining the general state of the art which is not considered to be of particular relevance
"D" document cited by the applicant in the international application
"E" earlier application or patent but published on or after the international filing date
"L" document which may throw doubts on priority claim(s) or which is cited to establish the publication date of another citation or other special reason (as specified)
"O" document referring to an oral disclosure, use, exhibition or other means
"P" document published prior to the international filing date but later than the priority date claimed
"T" later document published after the international filing date or priority date and not in conflict with the application but cited to understand the principle or theory underlying the invention
"X" document of particular relevance; the claimed invention cannot be considered novel or cannot be considered to involve an inventive step when the document is taken alone
"Y" document of particular relevance; the claimed invention cannot be considered to involve an inventive step when the document is combined with one or more other such documents, such combination being obvious to a person skilled in the art
"&" document member of the same patent family

Date of the actual completion of the international search	Date of mailing of the international search report
23 August 2019 (23.08.2019)	30 SEP 2019
Name and mailing address of the ISA/US Mail Stop PCT, Attn: ISA/US, Commissioner for Patents P.O. Box 1450, Alexandria, Virginia 22313-1450 Facsimile No. 571-273-8300	Authorized officer Shane Thomas Telephone No. PCT Helpdesk: 571-272-4300